University of Stavanger

Faculty of Science and Technology

MASTER'S THESIS

Study program/ Specialization:	Spring Semester, 2015
Petroleum Geosciences Engineering	Open Access

Writer:	
Gustavo de Carvalho Lopes	.... *(Writer's signature)*

Faculty supervisor: Chris Townsend

External supervisor: N/A

Thesis title:

Geological mapping of the south-central Gulf of Corinth coastal fault system - Greece

Credits (ECTS): 30

Key words:	
Greece, Gulf of Corinth, Normal Fault, Extensional Tectonics Rotated Fault Blocks, Half Graben Displacement, Depositional systems, Geological Mapping	**Total Pages:** 79 Stavanger, June, 2015

Geological mapping of the south-central Gulf of Corinth coastal fault system - Greece

By

Gustavo de Carvalho Lopes

Master Thesis

Presented to the Faculty of Science and Technology

University of Stavanger

University of Stavanger

June, 2015

ABSTRACT

This thesis is related to geological mapping of the south-central Gulf of Corinth (Greece), providing an interpretation for the major fault systems towards the east and the west of much studied coastal fault segments: Eghio, Eliki, Mamousia and Pirgaki.

The Corinth Rift is the focus of numerous studies witch are typically centered on key locations and relate to active coastal faults and syn-rift sediments. A structural framework that allows for data integration is of great importance, however regional structural studies have considerable impediments as fault scarps are frequently affected by erosional processes or covered by syn-rift sediments.

It is the main intention of this thesis to describe faults while investigating regional connectivity, linkage and continuity. Detailed descriptions of depositional systems are available on the literature, hence field observations intend only to aid fault characterization and contribute for an integrated regional perspective.

Field work covered over 1300 km^2, produced 312 observation points with over 500 field measurements. Over the course of 17 days, field activities strived to map and describe faults while observing lithological changes and comparing field data with literature information. Multispectral satellite compositions were designed for the purpose of geological and geomorphological compartmentalization, while gravimetric datasets and digital elevation models supported field mapping and discussions.

The regional scope of field mapping with the occasional impracticality of field observations, added to the different scales and uneven distribution of literature were major obstacles for this project. Nonetheless major fault zones have been defined as composed of multiple unaligned segments up to 10 kilometers long that connect over soft and hard linked structures to develop regional trends. These trends extend for up to 50 kilometers on a predominant S75°E direction and present lower displacement trend west and northwards. Segments have brittle fault damage zones up to 100 meters wide containing discrete fault surfaces marked with slickensides that suggest a mix of normal and oblique slip. The average of displacements estimates is 1530 meters with maximum 4700 and minimum at 230. Fault development in the region is an important factor controlling syn-rift depositional systems where modern examples can be used to predict expected patterns on older units in the study area.

ACKNOWLEDGEMENTS

TABLE OF CONTENTS

LIST OF FIGURES

LIST OF TABLES

INTRODUCTION

The master's thesis at University of Stavanger is a written report related to an independent project in which the knowledge accumulated during studies is applied. Field work provides a means to apply this knowledge while allowing to obtain a sense of spatial and temporal scale related to geological processes.

This project is situated in an active continental extension setting between the Peloponnese peninsula and mainland Greece (Figure 1). The southern shoulder of Gulf of Corinth has a land strip that is marked by a series of rotated fault blocks bounded by north-dipping normal faults (Skourtsos and Kranis, 2009).

The rotated fault blocks create half-graben structures that are infilled by alluvial, fluvial, lacustrine and deltaic facies that are divided into three major groups (Pavlides et al., 2003; Skourtsos and Kranis, 2009; Gobo, 2014b).

Figure 1 – Regional map showing the study area in context with Greece. Background image is composed of ArcMap World Imagery mosaic (Esri, 2014)

The active coastal faults and syn-rift sediments are frequent topics of study in the Corinth Rift, with only a few regional maps available presenting a simplified structural framework (Benedicto et al., 2008; Ford et al., 2009; Backert et al., 2010; Taylor et al., 2011). For this reason the main objective of project is to provide a structural framework interpretation of the south-central Gulf of Corinth.

To meet this thesis objective using 17 days of field work, it is important to integrate field data and remote sensor datasets with spatially dispersed literature sources of different scopes and scales. Together in an organized database, this knowledge can support the development of a comprehensive regional map that takes into account the information presented on former studies while updating this knowledge to the new data that has been acquired.

It is important to notice that the focus of this thesis is on normal fault mapping and characterization. Sedimentological field data was obtained, interpreted and discussed whenever possible. However it is not the intention of this thesis to provide a detailed description or evolution of the sedimentary units in the region.

With the described objectives set, the project will be presented into the following main sections:

- Geological Background – Starting with the structural and sedimentary framework used to approach this research with references to models and definitions, this section follows into a regional geology of the Hellenides with a description of the tectonic setting and evolution. To finalize, this section develops into a local geology description of the rift structures with a complete reference to the literature available, their main observations and conclusions.

- Methodology – Datasets will be detailed with procedures for each major phase being highlighted. Standards used for measurements and calculations will be presented, and a proposed geological map is defined. This map is part of the interpretation results but will be presented on this section to simplify the referencing as it is used as a base layer on many other images in this thesis.

- Observations – Pictures, locations, measurements, plots and maps will be shown and discussed in relation to patterns and structures they display. This section will start with a brief regional geomorphology and remote sensor compartmentalization, moving to detailed structural and lithological subsections.

- Interpretations and Discussions – Observations were used to generate interpretations that are often not singular for a given problem. Discussions are then presented to evaluate and suggest the best fit solution for the given observations and datasets available. To finalize this section, profiles and displacements are calculated and analyzed based on interpreted best fit solutions.

- Conclusions – A summary of the thesis, with focus on interpretations and discussions.

GEOLOGICAL BACKGROUND

STRUCTURAL AND SEDIMENTARY FRAMEWORK

Before discussing the complexity of fault segment interaction, it is important to define and describe a single fault. Faults are fractures across which there is rock displacement parallel to the fracture plane (Gudmundsson et al., 2013). The displacement field of a single isolated fault can be idealized as an ellipse, where the maximum displacement occurs at the center of the surface and diminishes toward the edges creating a symmetric displacement versus fault length (D-L) profile as shown on Figure 2 (Doutsos and Koukouvelas, 1998; Gawthorpe and Leeder, 2000). For adjacent fault segments the D-L profiles can be asymmetric indicating mechanical interaction, and suggesting that an array of segments may essentially act as a single fault(Figure 2) (Gawthorpe and Leeder, 2000).
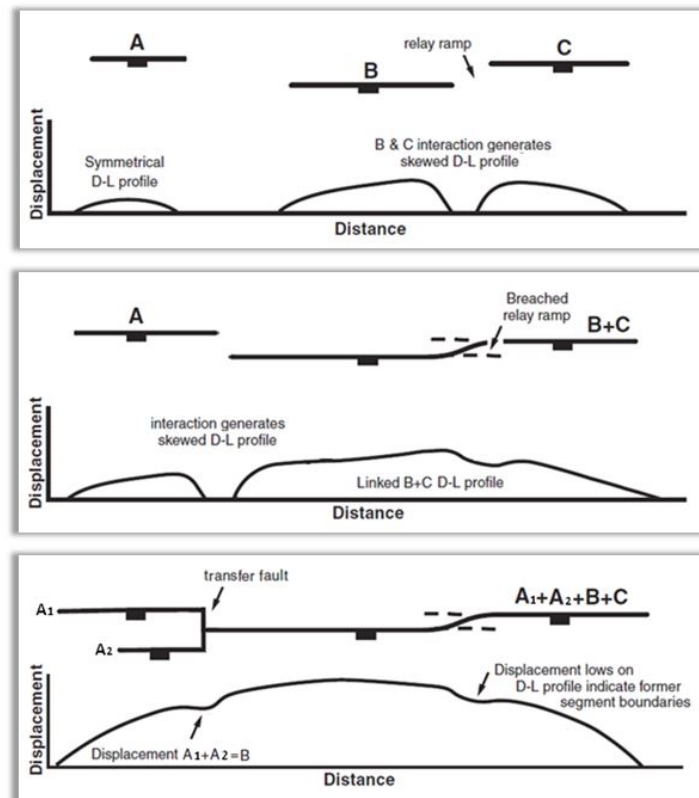
Figure 2 - Schematic evolution of a major fault zone composed of segments, showing displacement versus fault length (D-L) profiles modified from Gawthorpe and Leeder (2000). Segments A, B and C show from top to bottom the fault initiation stage transitioning to interaction and linkage stages on bottom images. Transfer zones and transfer faults are represented.

Major faults rarely develop as isolated structures, but are commonly related to fault segments that grow and interact either over transfer zones or transfer faults (Etheridge, 1986; Morley et al., 1990; Gawthorpe and Leeder, 2000; Acocella et al., 2005). Cowie (1998) advocates that fault growth starts with a nucleation phase, composed of isolated sub-parallel and scattered segments, that

5

either develop into major fault zones or become inactive as the deformation progressively becomes localized (Figure 3).
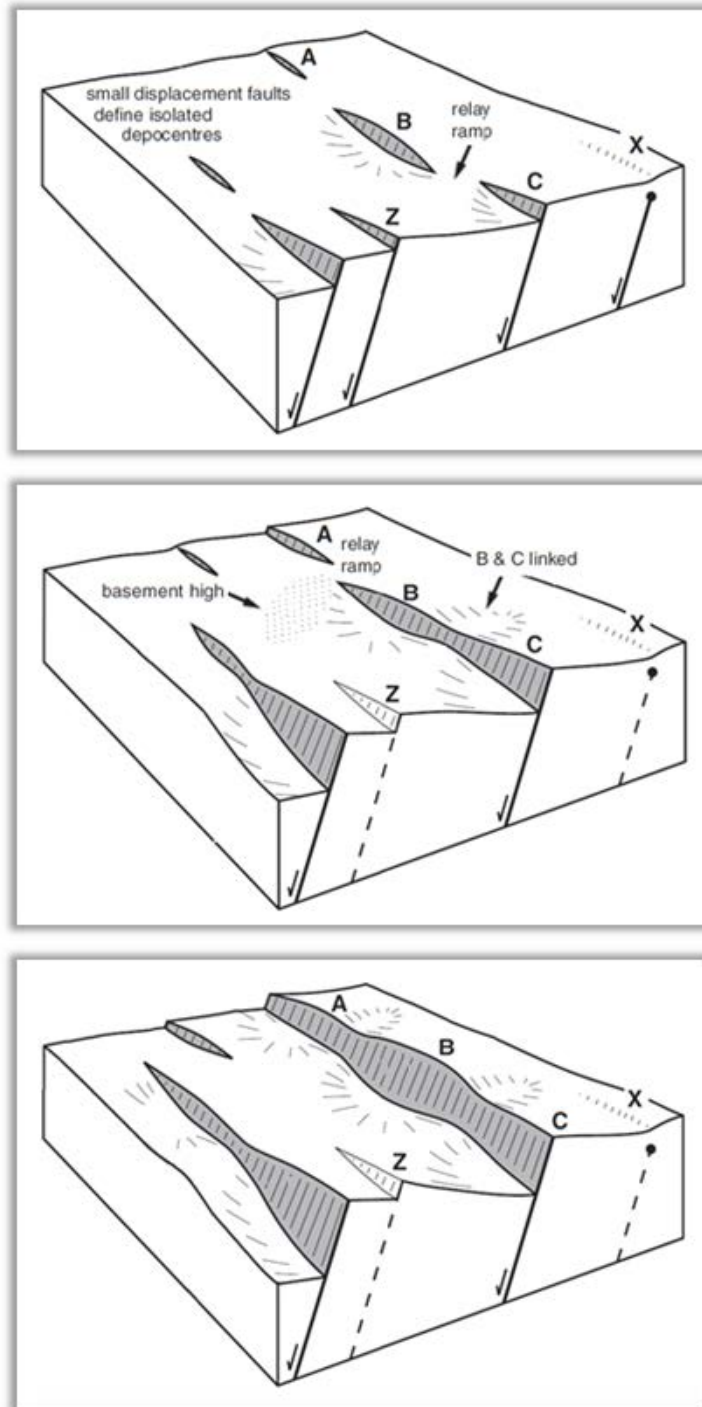
Figure 3 - Schematic 3D evolution of a normal fault array modified from Gawthorpe and Leeder (2000). First image illustrates the fault initiation stage, and is characterized by a large number of small-displacement normal fault segments. The following two images illustrate the fault interaction and linkage stage, showing how deformation in the fault array becomes localized along major fault zones (A, B, C), and faults located in stress shadows begin to become inactive (X, Z). The X denotes a monocline above a blind fault tip. Grey and white segments denote respectively active and inactive faults.

The term fault zone is commonly used on the literature to denote one single main core fault and a damage zone associated to it (Gudmundsson et al., 2013). On this thesis the term fault zone will be

6

extended to describe also a regional group of parallel and interacting fault segments that are aligned on a regional lineament trend which concentrates the extensional deformation (Figure 4) (Peacock et al., 2000). It is important to note as well that the term fault zone may be used interchangeably with the term fault depending on the scale of observation.
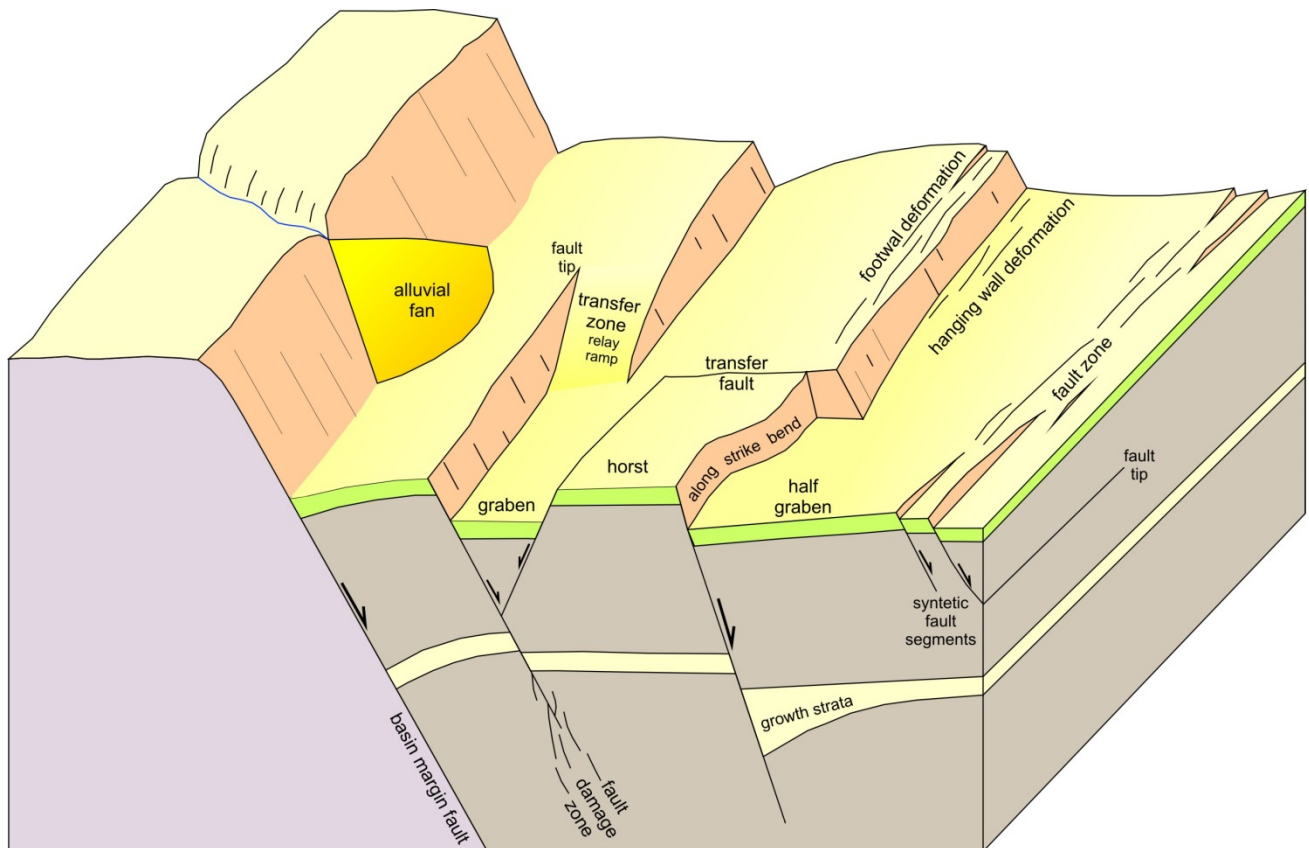
Figure 4 - Schematic block diagram showing the main geometric features of normal faults and their relation to sedimentary structures and basin evolution. This figure has been simplified from Peacock et al. (2000) with extra classifications from Morley et al. (1990) to cover notations and nomenclature terms used on this thesis.

As mentioned previously, fault segments interact and link mainly over transfer zones or transfer faults, these structures are exemplified on Figure 4 (Etheridge, 1986; Morley et al., 1990; Gawthorpe and Leeder, 2000; Acocella et al., 2005). It has been suggested by experimental data that transfer zones are predominant on systems where distention is low (<16%), while transfer faults are more commonly found where there is significant stretching (>39%) (Acocella et al., 2005).

Passive margins, wide rifts and back-arc basins are settings where transfer faults are commonly described. These faults (Figure 2 and Figure 3) are sub-vertical transtensive structures that transfer the displacement between adjacent crustal sectors undergoing extension (Etheridge, 1986; McClay and Khalil, 1998; Acocella et al., 2005). It is important to note that transfer faults are commonly lacking within continental rifts (Acocella et al., 2005).

Transfer zones on the other hand are frequent on extensional systems where there is low stretching, and develop as a group of deformational features that attempt to conserve the regional strain between fault segments (Morley et al., 1990; Peacock, 2002; Athmer and Luthi, 2011). These zones can significantly influenciate the development of normal faults, with relay ramps being the most common structure of the kind (Figure 2, Figure 3 and Figure 4) (Peacock, 2002). Although transfer zones are not initially developed as hard link structures, as the strain increases the transfer zones may breach creating a hard link between segments (Giba et al., 2012). McClay and Khalil (1998) classify these breached relay ramps as small transfer faults.

With the development and linkage of fault segments on extensional basins there is the formation of half grabens and rotated fault blocks, all of which influenciate sedimentation paths and processes (Athmer and Luthi, 2011). A development model for such environment is described by Gawthorpe and Leeder (2000), and can be summarized on the following four steps shown on Figure 3:

1. While on the nucleation phase described by Cowie (1998) there is the development of many fault bounded basins;

2. As faults start to dominate the landscape either the new topography causes river deflection, or antecedent drainages erode rising foot wall blocks creating;

3. Rift segments start as topographically closed systems with lakes being common features of these structurally isolated half grabens;

4. With fault development and increase of relief, short narrow drainage basins develop with rapid deposition of alluvial fans and fan deltas;

5. With the development of major fault zones by progressive segment interaction, sediments from linked depocentres may be reworked and incised to create an elongated half graben basin, typified by the Gulf of Corinth (Gawthorpe and Leeder, 2000).
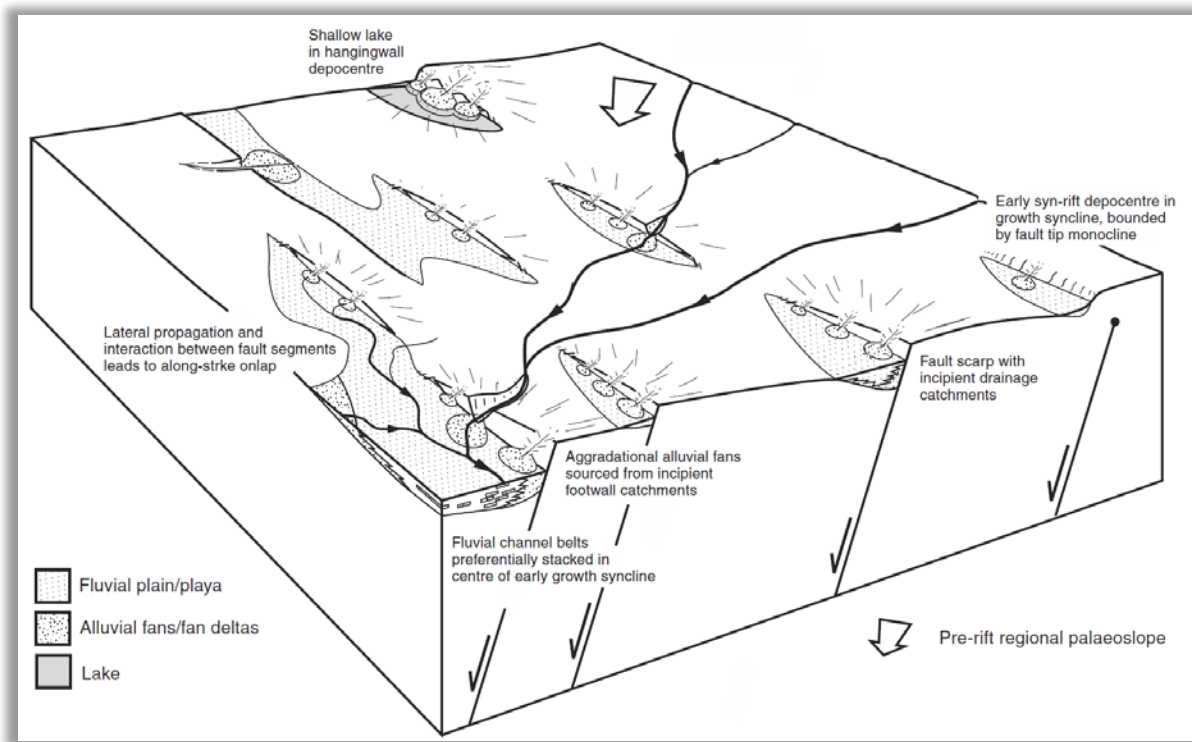
Figure 5 - Tectonosedimentary evolution of a normal fault array on continental environments modified from Gawthorpe and Leeder (2000).

REGIONAL GEOLOGY

The Hellenides comprise of a northwest trending orogenic system that accommodates a northeast dipping subduction zone of Ionian seafloor along the Hellenic trench (Papanikolaou and Royden, 2007).

Several tectonic and paleogeographic models of the Hellenides have been proposed involving a different number of basins, terranes and geodynamic settings. Papanikolaou (2013) proposes a model with the distinction of nine terranes (Figure 6).
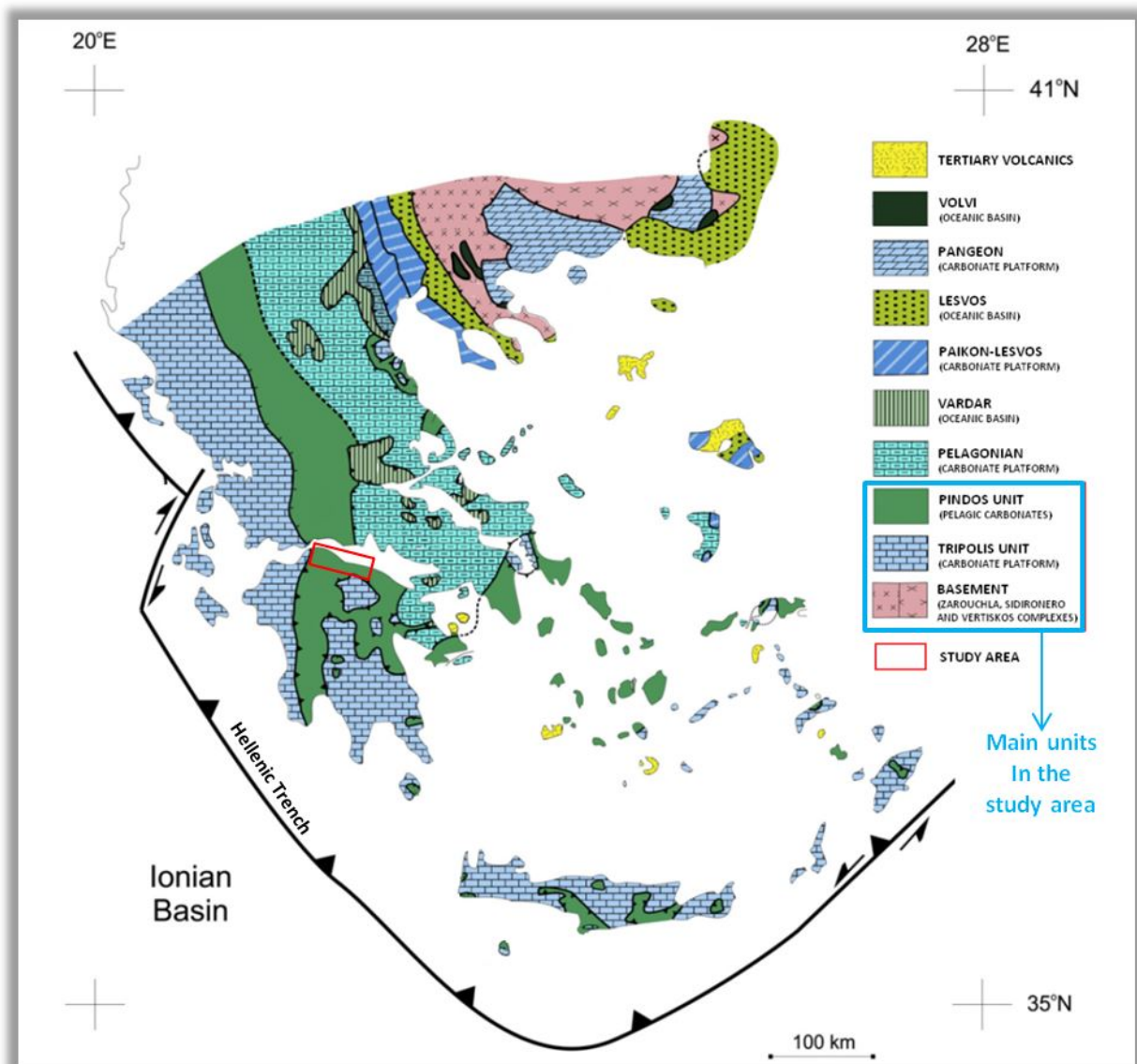
Figure 6 - Terrane map of the Hellenides modified from Papanikolaou (2013).

Each terrane of Figure 6 is defined as a dynamically evolving element undergoing distinct paleogeodynamic and paleogeographic evolutions, all of which can be simplified by three major stages:

I.   Continental rifting in the northern margin of Gondwana on the Late Paleozoic–Triassic;
II. Oceanic opening in between the continental terranes during Triassic–Paleogene;
III. Accretion of the terranes with docking along the active European margin from Jurassic to Neogene.

Thrusting on the accretion stage has resulted in the stacking of a nappe pile, that on the northern Peloponnesus area is composed mainly of three different tectonostratigraphic units (Figure 6): the Zarouchla complex composed of phyllites and quartzites, which is overthrusted by the Tripolis neritic and platform limestone's, which is in turn overthrusted by the Pindos pelagic limestone's and flysch deposits (Figure 6) (Skourlis and Doutsos, 2003; Papanikolaou and Royden, 2007; Benedicto et al., 2008; Ford et al., 2013).

Extension in the Hellenides is described by Papanikolaou and Royden (2007) as starting on the Oligocene and lasting until the Quaternary. The first indications of extension are perpendicular to the Hellenides northwest structural trend, while towards the late Pliocene extension directions transitionally rotate to a north-south direction to superimposes and crosscuts Hellenide thrust sheets, developing among other structures the Corinth Rift (Ford et al., 2013; Papanikolaou, 2013).

LOCAL GEOLOGY

The Corinth Rift is a WNW–ESE extensional basin, which separates central mainland Greece from Peloponnese peninsula. The rift can be described as a composite asymmetric graben with varying geometry along strike. Its northern portion is lying mainly offshore, while the southern shoulder has an approximate 20km wide land strip characterized by a series of rotated fault blocks bounded by north-dipping normal faults (Skourtsos and Kranis, 2009).

The rotated fault blocks create half-graben structures that are infilled by syn-rift deposits characterized by three main groups (Pavlides et al., 2003; Skourtsos and Kranis, 2009; Gobo, 2014b):

- The Lower Group is defined mainly by 1000-2000 meters of fluvial-lacustrine facies associated with alluvial sediments that are developed at the initial stages of the rift.
- The Middle Group is characterized by up to 1200 meters of northward prograding giant Gilbert type deltas composed of a mix of coarse sediment and fine grained turbidites.
- The Upper Group embraces at least two recent depositional systems along the current coast line, one composed by a series of marine terraces and other by modern Gilbert type deltas (Gobo, 2014b).

The Lower Group deposits are dominant on the south, while Lower, Middle and Upper groups share influence on the north towards the modern coast line (Figure 7) (Benedicto et al., 2008; Ford et al., 2013; Gobo, 2014b).

The rift age is poorly constrained, with recent data sources suggesting that extension has taken place from Plio-Pleistocene to recent (Leeder et al., 2008; Ford et al., 2013; Hemelsdaël and Ford, 2015). The western portion of the rift presents higher extension rates than the eastern, and although located entirely on an extending domain, the syn-rift sediments on the southern margin of the rift have been uplifted 1800 meters were the driving mechanism is poorly understood (Skourtsos and Kranis, 2009; Hemelsdaël and Ford, 2015).

This thesis covers the southern shoulder of the rift where the main faults, from south to north, are the Mamousia-Pirgaki, Eliki and Eghio faults (Figure 7). These faults have different levels of seismic activity and are progressively younger towards the north, with planes dipping 45 to 70° (Pavlides et al., 2003; Cornet et al., 2004; Daniel et al., 2004; De Martini et al., 2004; Géraud et al., 2006; Micarelli et al., 2006; McNeill et al., 2007; Leeder et al., 2008).
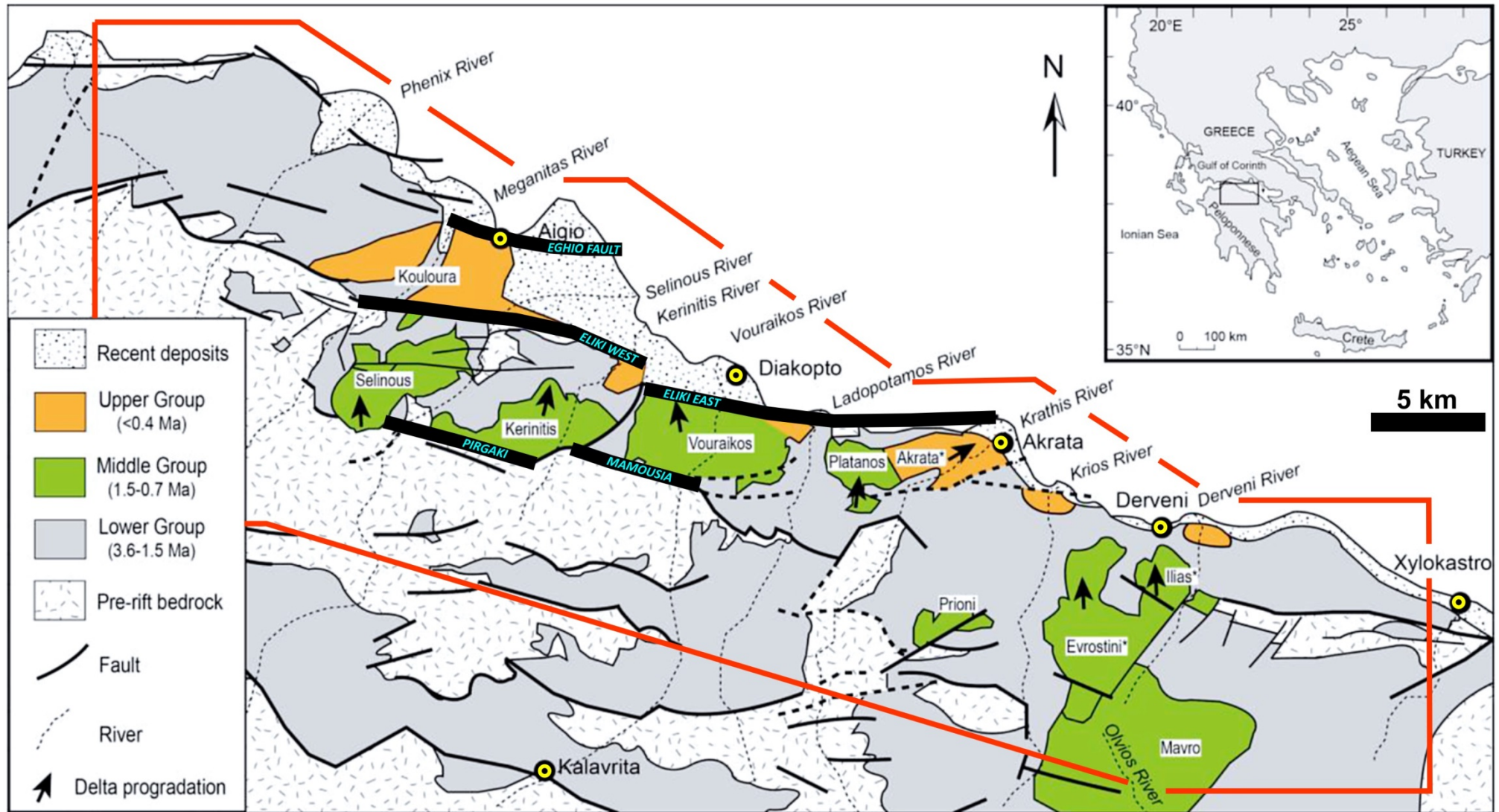
Figure 7 – Local geological map modified from: (Ford et al., 2009; Backert et al., 2010; Gobo, 2014b). Red contour defines the extent of the study area. Recent deposits and Upper Group are Gilbert type deltas and marine terraces; the Lower group is defined as fluvial lacustrine deposits; pre-rift bedrock is defined as the basement for this project and is composed mainly of undifferentiated carbonates. Main faults described in the area are highlighted with bold lines (Eghio, Eliki and Mamousia-Pirgaki).

13

Faults in the region are generally named after the main city or village located on the proximity of the fault line.

The Mamousia-Pirgaki Fault is the southernmost structure that has been investigated in detail on the area of interest. It is described as a mature fault developed at the beginning of the Corinth Rift, and is composed of at least two north dipping and left stepping normal fault segments separated by the Kerinitis River (Hatzfeld et al., 2000; Skourtsos and Kranis, 2009; Ford et al., 2013). The mechanism connecting the Mamousia and Pirgaki segments is not discussed in detail on the literature although maps with interpretations are commonly presented (Ford et al., 2009; Backert et al., 2010) (Figure 7). The Mamousia segment is located to the east and does not present fault surface exposures described on the literature, but its topographical expression and the observable lithological changes have supported map interpretations. The Pirgaki segment is located to the west and is described by Micarelli et al. (2003) and Micarelli et al. (2006) with a maximum elevation of 1778 meters, presenting multiple fault surface exposures with N095-100° strike and a 40-70° dip. These fault exposures are defined with a continuous fault scarp of up to 300 meters, and an observable fault damage zone ≈ 50 meters thick.

The Mamousia-Pirgaki Fault defines the southern border of a rotated fault block that is, from west to east, infilled with the Selinous, Kerinitis and Vouraikos uplifted Gilbert-type deltas of the Middle Group, overlaying the less exposed Lower Group lithologies (Figure 7). The fault block is bounded northward by the Eliki Fault.

The Eliki Fault is described as two right stepping and north dipping normal fault segments separated by the Kerinitis River. Mrlina (2014) indicates a transfer fault linkage while McNeill and Collier (2004) describe a transfer zone as the link mechanism. The Eliki West and Eliki East segments display an average N100° strike with a 55-65° dip and differ on morphological and tectonic aspects (Pavlides et al., 2003; Micarelli et al., 2006). Literature defines the western segment with a maximum elevation of 485 meters, presenting a fault damage zone of ≈ 100 meters, where exposed footwall juxtaposes more than 5 kilometers of its length with basement carbonates. The eastern segment on the other hand presents a higher maximum elevation with 721 meters, a wider fault damage zone of almost 400 meters, and juxtaposes only Middle Group sediments on its fault scarp (Koukouvelas et al., 2001; Micarelli et al., 2003; Pavlides et al., 2003). With a constant 5 millimeters/year slip rate and a deduced displacement of 650 to 800 meters, the fault age is

estimated around 130.000 years (Pavlides et al., 2003; Micarelli et al., 2006).

The Eliki Fault defines the southern border of a rotated fault block bounded by the Eghio Fault to the north. This block is infilled from west to east by the uplifted Koulouris Delta and the modern Eghio and Diakopto deltas (Figure 7) (Gobo, 2014a).

The Eghio Fault is one of the youngest major normal faults in the Gulf of Corinth with fault scarp that is approximately 100 meters high juxtaposing unconsolidated conglomerates. The fault is trending N100° with a northward 60° dip, a throw of approximately 200 meters, and an estimated age of about 60.000 years assuming a constant slip rate of 3 millimeters/year (Micarelli et al., 2006; McNeill et al., 2007; Place et al., 2007). The Eghio Fault decreases its displacement towards the east and the main structure is believed to terminate close to the current course to the Meganitis River (Micarelli et al., 2006; McNeill et al., 2007). Besides the main Eghio Fault, the Eghio Fault Zone is described as multiple subparallel segments visible on satellite and bathymetric data (McNeill et al., 2007).

The syn rift sediments in the southern shoulder of the Gulf of Corinth lay over a complex tectonically derived pre-rift substratum that is well represented by tree main units on the northern Peloponnesus: the Zarouchla complex, the Tripolis and Pindos units. The dominant pre-rift unit in the study area is the Pindos thrust sheet (Figure 6) (Skourlis and Doutsos, 2003; Benedicto et al., 2008; Ford et al., 2013). All the pre-rift tectonic units are treated as a single undifferentiated basement for the purpose of this thesis.

DATA AND APPLIED METHODS

Pre-Field Work

The focus prior to the field has been on optimizing the 17 days of field work to cover adequately the approximate 1300 km^2 of the project area. To achieve this goal, several datasets were brought into the ArcMap GIS platform (Esri, 2012) and compared with geological interpretations extracted from georeferenced maps available on the literature (Figure 8).
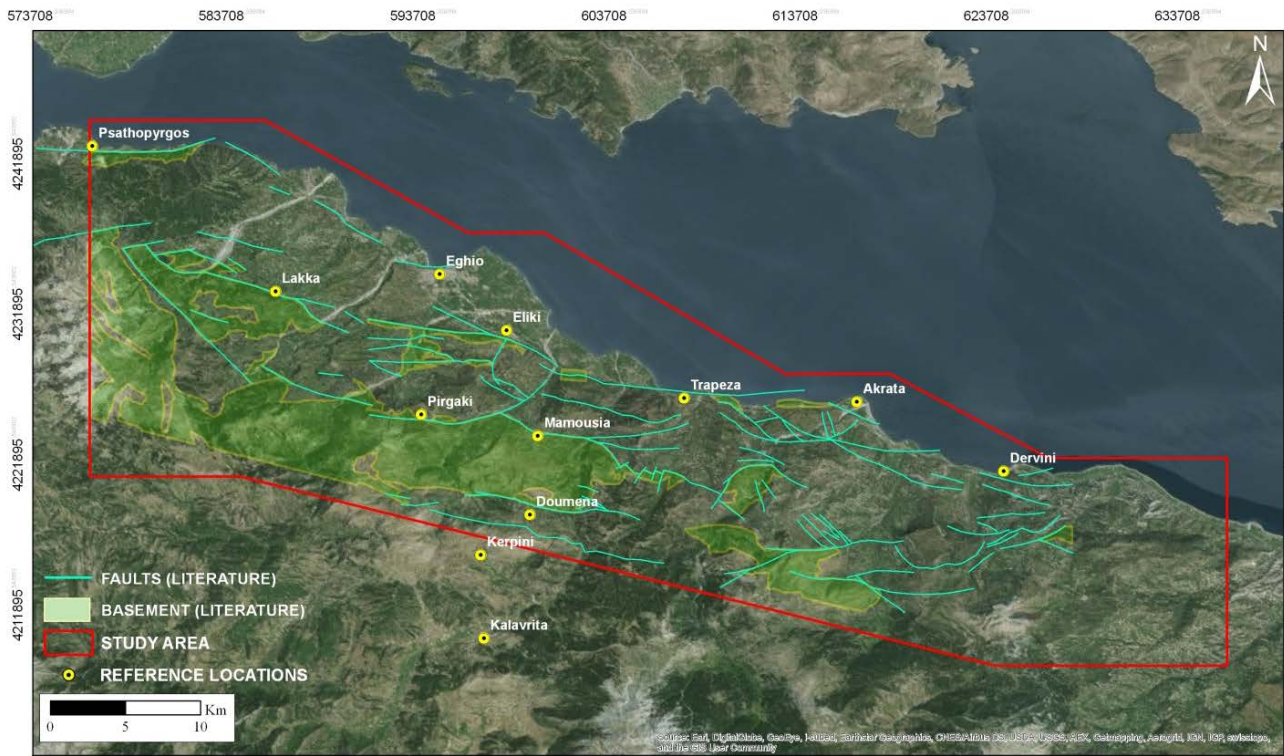
Figure 8 – Local map of the study area showing the compilation of data found in the literature (McNeill and Collier, 2004; Flotté et al., 2005; Ghisetti and Vezzani, 2005; McNeill et al., 2005; McNeill et al., 2007; Rettenmaier, 2007; Rohais et al., 2007; Benedicto et al., 2008; Ford et al., 2009; Backert et al., 2010; Leeder et al., 2012; Ford et al., 2013; Gobo, 2014b). Represented faults are predominantly north dipping structures and the basement in the area consists mainly of undifferentiated carbonates that are covered by syn rift deposits (Skourtsos and Kranis, 2009). Background image is composed of ArcMap World Imagery mosaic (Esri, 2014).

Published work in the study area shows emphasis on sedimentological observations, and is concentrated on the area of Eghio, Eliki, Pirgaki and Mamousia, while to the west and east of this central area fewer papers are available. To the east of Dervini there is a gap where no publications were found.

Given the difference on scales and uneven distribution of the information available in the area, regional datasets were used to bring consistency to the work; these will be described in detail on the following points:

1. SATELLITE IMAGERY

Landsat 8 OLI/TIRS satellite (USGS, 2014) was used as it has a good balance between spatial and spectral resolutions, presents good coverage and periodicity allowing the selection of recent scenes with low cloud coverage, and it is available without cost for study purposes.

The Landsat 8 contains 11 bands. The Operational Land Imager (OLI) sensor produces 8 multispectral bands with 30 meters of spatial resolution, and 1 panchromatic band with 15 meters of spatial resolution. The Thermal Infrared Sensor (TIRS) produces 2 multispectral bands with 100 meters of spatial resolution. Each of the 11 bands can be assigned to a red, blue or green channel creating a digital RGB image that can be visualized on a GIS platform.

Bands 1, 5 and 9 are not adequate for geology, being specifically designed to map the atmosphere, water or vegetation. With the permutation of the remaining 9 bands it is possible to create 504 different images, so reflectance curves were analyzed to find specific combinations that show contrast between carbonates and clay minerals (Figure 9). This contrast might relate to basement and sedimentary cover areas in the study area, producing images that might relate to geological boundaries.
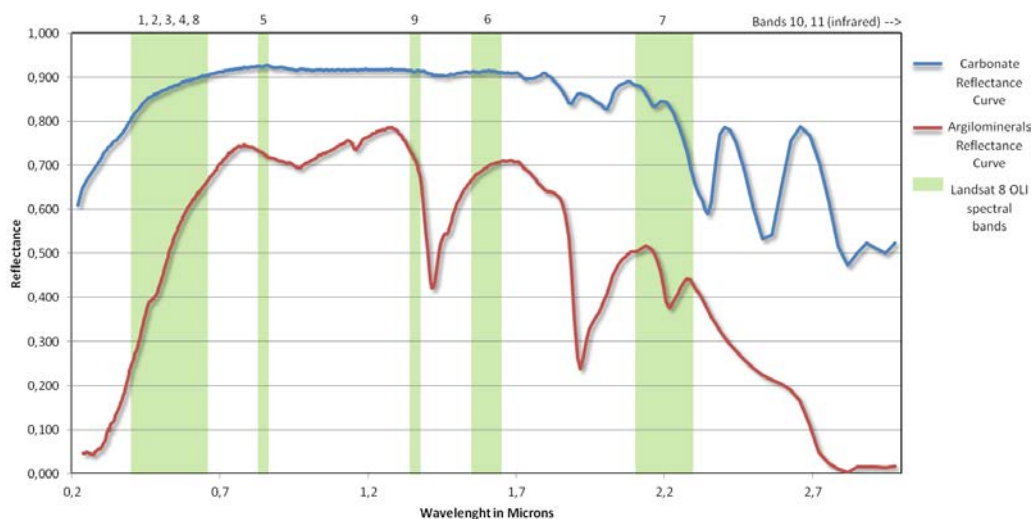
Figure 9 - Plot of reflectance versus wavelength for an idealized carbonate rock (blue) and average clay minerals related to sedimentary covers (red). Green areas represent Landsat 8 OLI sensor spectral bands. The TRIS sensor covers the thermal infrared (high wavelengths) and is not directly overlap with the mineral reflectance curves. Plotted data was obtained on USGS reflectance library (USGS, 2014).

After evaluating band combinations in relation to areas of known geological units, the RGB composition 6-4-10 was defined adequate to support the geological interpretation of the study area (Figure 10)
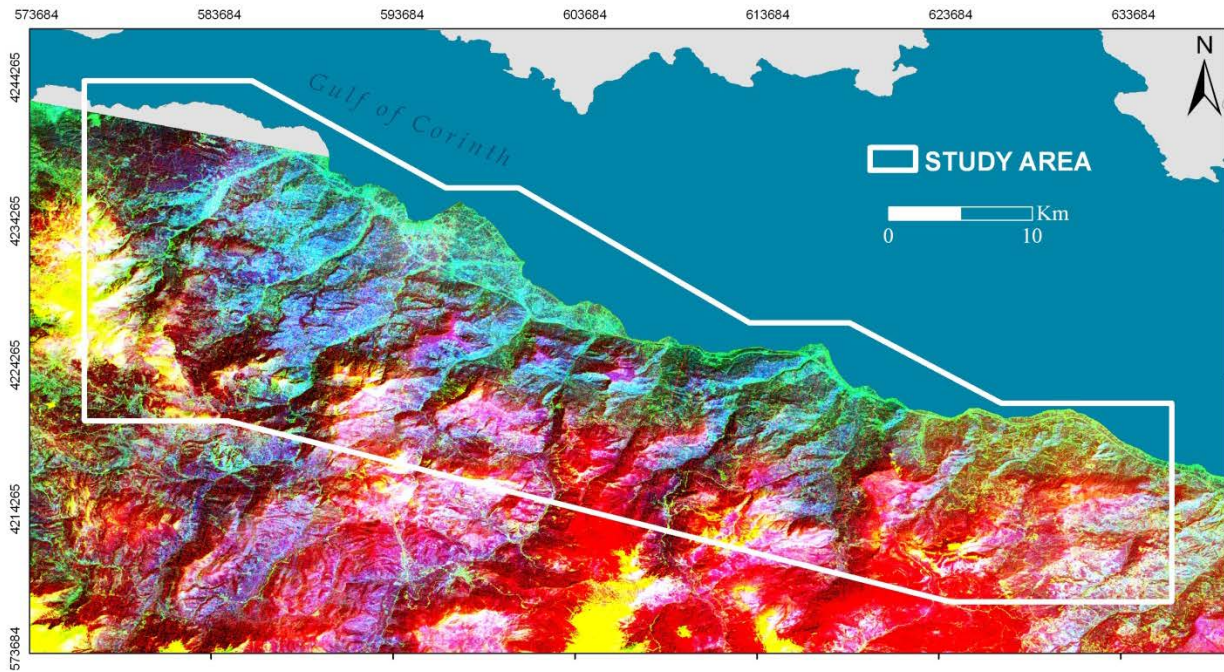
Figure 10 - Landsat 8 OLI/TIRS scene with RGB composition 6-4-10. Band 6 represents the shortwave infrared and is particularly efficient on differentiating rocks and soils that have different reflectance patterns on its range, band 4 is on the red spectrum and is adequate to define land use, and band 10 is on the thermal infrared wavelength and brings information about the ground temperature witch might relate to different lithologies. Vegetation is mapped well with bands 6 and 10 and therefore interpretation should take this into account

To eliminate redundancy of variance due to terrain slope, elevation and other factors, a principal component transform was performed and the resulting image showed a good accuracy on discriminating different lithologies.
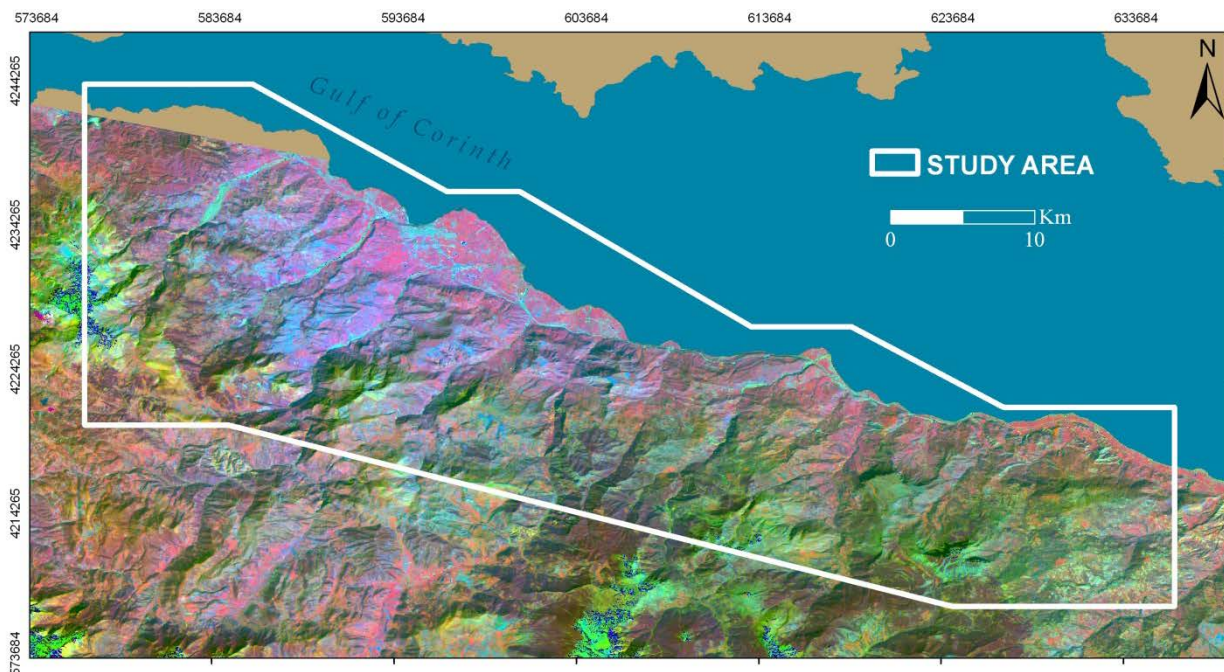
Figure 11 – Principal Component scene of Landsat 8 OLI/TIRS RGB composition 4-2-6. Band 4 is on the red spectrum and is adequate to define land use; Band 2 is on the visible blue spectrum; Band 6 represents the shortwave infrared and is particularly efficient on differentiating rocks and soils that have different reflectance (USGS, 2014).

19

2.   DEM (Digital Elevation Model)

The ASTER Global DEM data (USGS-METI, 2011) will be used as It has the highest resolution (1 arc-second spatial resolution representing approximately 30 meters), and is a free dataset for academic use (Figure 12).
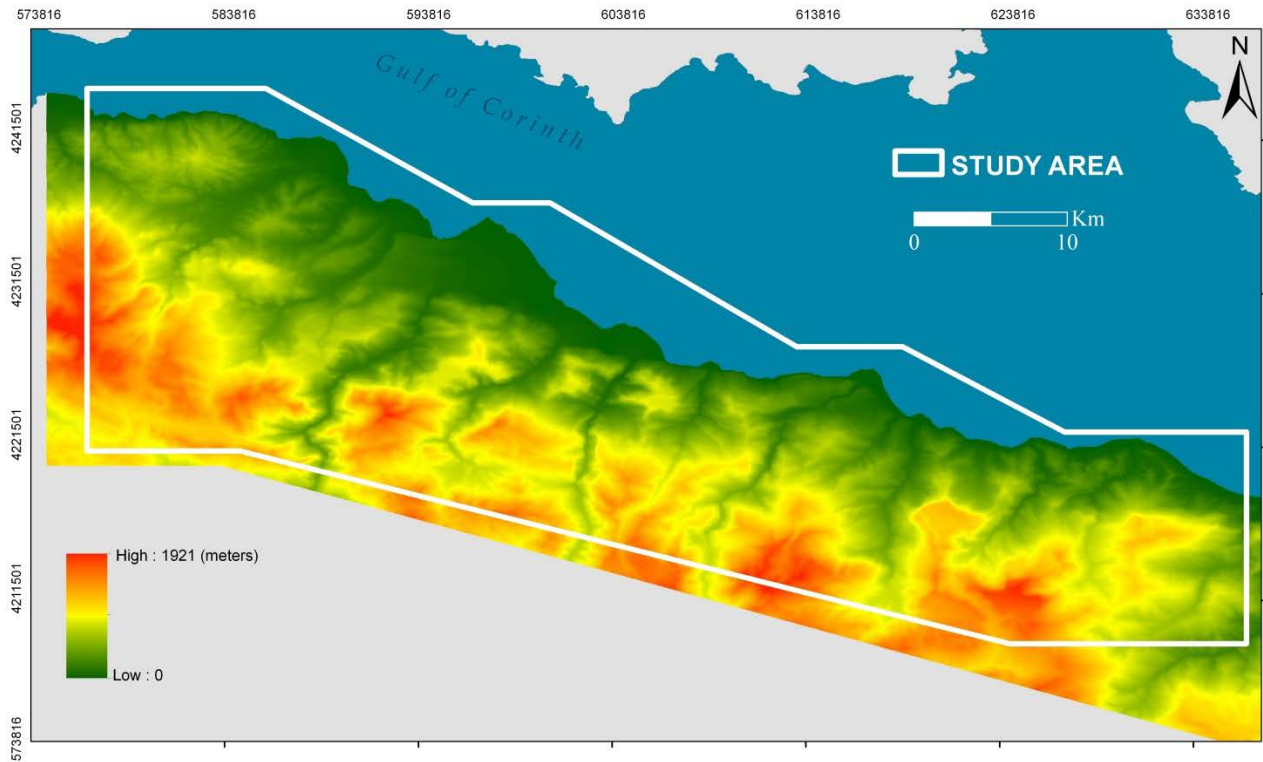
Figure 12 - ASTER Global DEM (USGS-METI, 2011) raster data on a GIS platform with approximately 30m spatial resolution, showing elevations from sea level to 1921 meters above sea level in the study area.

Other commonly used source of DEM is within the image mosaic (Google, 2015b) available in the Google Earth Pro software (Google, 2015a). This DEM is associated with multiple high resolution satellite images and therefore is a useful tool. Precision and georeferencing are questionable within this software, and therefore all evaluations and values were quality controlled with the ASTER Global DEM data (USGS-METI, 2011) using ArcMap (Esri, 2012).

3.   GRAVITY

Gravity models are powerful tools for mapping tectonic structures that are buried under sediment cover, but there are many discrepancies between measured and theoretical gravity fields. The correction for measurement altitude and latitude is known as "free air", and for the topographical masses above or below a datum is called "Bouguer". (Sandwell et al., 2014)

GGMplus World Gravity Data (WACG, 2014) is a recent dataset that provides models of Earth's "free air" corrected gravity with a 200 meter spatial resolution in the study area. Topographical mass differences are present on this dataset (Figure 12), and therefore any interpretation has to be done in association with a DEM. Although no Bouguer correction has been performed, the GGMplus gravity maps (Figure 13) support regional geological interpretations at spatial scales above 10 kilometers (Hirt et al., 2013).

Mrlina (2014) presents a free-air and Bouguer corrected gravity dataset filtered to highlight fault density contrasts. The dataset covers only the center portion of the area of this thesis (Figure 13).
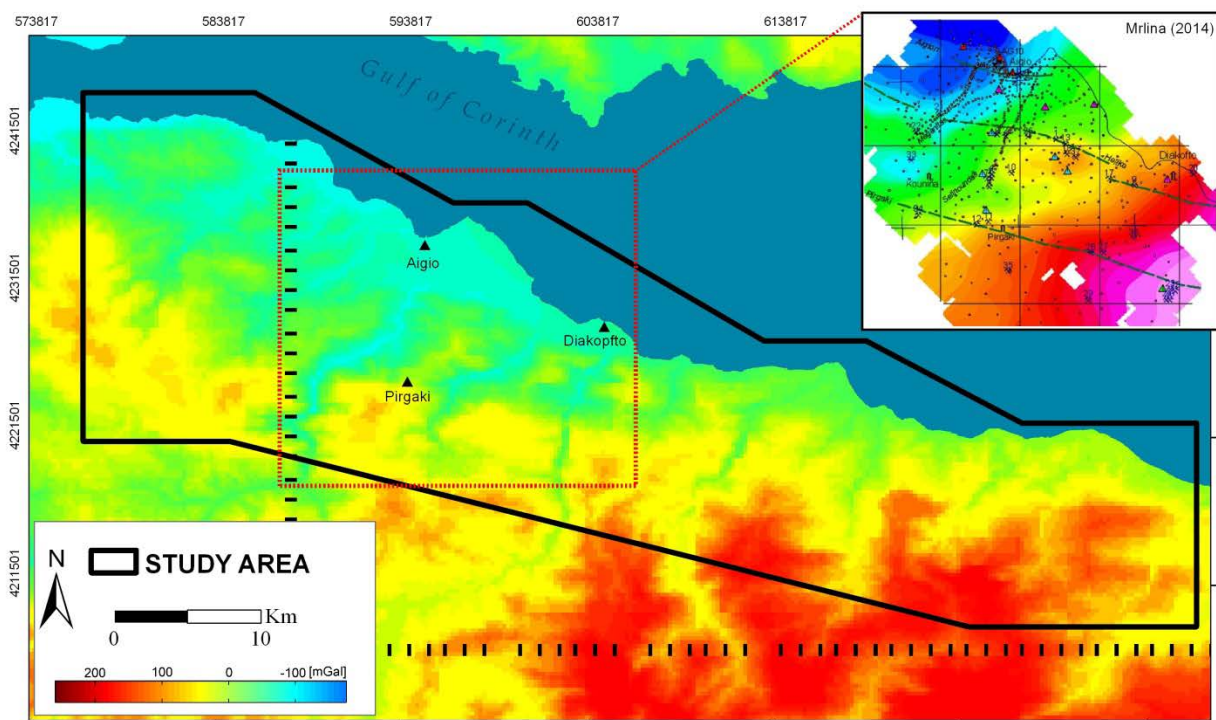
Figure 13 - GGMplus World Gravity (WACG, 2014) displaying the Gravity Disturbance functional in mGal. Gravity effects related to topographic mass are present and limit interpretations at spatial scales of less than 10 kilometers (Hirt et al., 2013). The highlighted square that covers a fraction of the area has a free-air and Bouguer corrected dataset shown on the corner image (Mrlina, 2014).

Field Mapping

The focus of the field work was to obtain adequate coverage of the approximate 1200 km^2 of the project area in 13 effective days of work. To achieve this goal field observations had to be limited to the vicinities of roads. During this project 1100 kilometers were driven and 312 observation points were mapped (Figure 14).

Figure 14 - Sketch of a map with observation points and driven paths.

Of the 312 mapped points, 16 were related to fault exposures and the remaining were related to unconformities and changes of lithology (Figure 15).

Georeferenced interpretations resulting from publications (Figure 8) were grouped, with information related to basement exposures and fault locations being printed as semitransparent layers over topographical maps. With this methodology all collected interpretations were taken to the field and evaluated on a day to day basis.

Literature data also aided the effectiveness of field work by allowing defining preferred investigation areas, which were then judged using remote sensor datasets in relation to outcrop exposure potential and accessibility. Favored study locations were defined by analyzing areas where literature mapped structures were consistent on multiple maps in relation to where they differed or were lacking altogether. By aiming for the areas where information was lacking on conflicting, and by evaluating the outcrop exposure probability and field accessibility, work could be

planned to aid the construction of a solid regional interpretation.

Driving routes were always defined based on accessibility, time constrains and the pre-field work datasets. After each day, data was integrated and reevaluated so that plans were constantly updated based on a daily progress.

Supported by the objective and scale of this thesis, the focus of field observations was concentrated on mapping and characterizing faults and unconformities. Simplified lithological description and compartmentalization is essential for any geological mapping and was done on all the investigated areas.

Fault exposures whenever uncovered and accessible were measured in detail with the objective of accounting for the strike and dip variability on every occasion these were visible on an outcrop scale. Slickenside lineation's as described by Doblas et al. (1997) were measured when clearly identifiable with care to define their relation with the dip directions being measured.

Unconformities are rarely exposed on outcrop scale and were mostly defined by observing lithological changes within two separate outcrop locations. Observations of the terrain and topography have been used to distinguish these lithological variations from fault related to unconformity related, where fault tend to create a clear topographical expression.

Due to the difficulty of obtaining statistically significant measurements, unconformities have been simplified as flat surfaces that are sub-parallel to the overlying syn-rift sediment layers. This is purely an assumption to support displacement calculations, as clear field observations over this surface are commonly not available.

Given the uncertainty related to the unconformity surface geometry, displacement value reliability depends upon the regional level of complexity this surface actually contains.

Whenever Lower Group sediments are not observable in a certain area, the Middle Group topsets were measured as a possible close approximation to the unconformity surface.

Post-Field Work

Field observation points as presented on Figure 14 are limited by time and accessibility. The number and uneven distribution of data points compared to the scale of the mapped area can be compensated by the diversity of regional datasets such as Landsat compositions (Figure 10 and Figure 11), digital elevation models (Figure 12) and gravity (Figure 13). These datasets are correlated with field data points, allowing for consistency of interpretation within areas where direct observations are not available.

Field observations are brought into ArcMap (Esri, 2012) and Google Earth Pro (Google, 2015a) where a comparison is done between literature based pre-field map (Figure 8) and field data related to syn-rift distribution, basement exposures and fault locations (Figure 15).
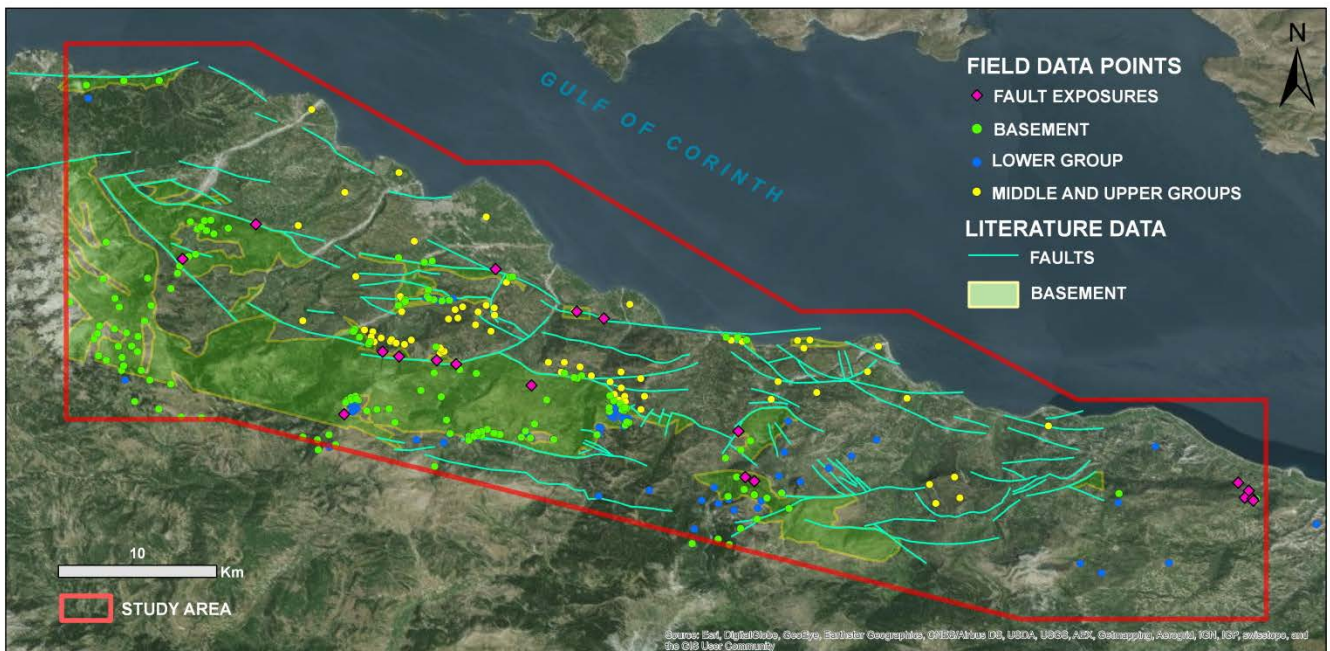
Figure 15 – Sketch map highlighting differences between local map shown on Figure 7 with field points where sediments of the Lower, Middle and Upper groups were mapped. Base map modified from: (Ford et al., 2009; Backert et al., 2010; Gobo, 2014b)

An updated geological map has been produced based on regional datasets (Figure 10, Figure 11, Figure 12 and Figure 13), field data (Figure 15), and the amalgamation and correction of key literature data (McNeill and Collier, 2004; Flotté et al., 2005; Ghisetti and Vezzani, 2005; McNeill et al., 2005; McNeill et al., 2007; Rettenmaier, 2007; Rohais et al., 2007; Benedicto et al., 2008; Ford et al., 2009; Backert et al., 2010; Leeder et al., 2012; Ford et al., 2013; Gobo, 2014b). To develop the final interpretation (Figure 16) the following decisions and procedures were taken:

    A. Upper Group and Middle Group lithological boundaries were mostly adopted from Ford et al.

(2009), Backert et al. (2010) and Gobo (2014a). Changes were adopted only where contradicting observation points were present (Figure 15).

B. Delta nomenclature from Upper and Middle groups were adopted from Ford et al. (2009), Backert et al. (2010) and Gobo (2014a).

C. Lower Group lithological boundaries were mainly interpreted from field observation points in association with Landsat 8 compositions (Figure 10 and Figure 11). Interpretations from all key literature papers are taken into account for areas where observations are not available.

D. Basement unit (also called pre-rift) is displayed as four different units. These have not been differentiated in the field and classification has been adopted from literature maps (Benedicto et al., 2008; Papanikolaou, 2013; Hemelsdaël and Ford, 2015)

E. Fault nomenclature and naming convention were adopted from key literature papers.

F. Although fault nomenclature has been adopted, fault traces were entirely interpreted using field data in association with remote sensor datasets available. Key literature data has been consulted and taken into account, but due to the lack of insight on how faults traces were defined, to keep consistency no fault traces were adopted from literature.

G. Fault interpretation is locally faithful to fault exposure field location and characteristics.

H. Faults are shown mostly as independent segments, as linkage of key segments is controversial and interpretations are discussed further on this thesis.

I. Fault dip direction is shown on major faults where topographical expression and fault surfaces where exposed. All other faults are left undefined.

J. Eghio Fault eastern offshore continuation is derived from bathymetric data present by McNeill et al. (2007).

K. Offshore and the northern coastal faults are representative simplifications based on maps from Koukouvelas et al. (2001) and Moretti et al. (2003)

L. Plotted measurements represent local trends where representative outcrops are visible. These measurements contribute for, but do not represent regional trends for each group as will be discussed further on this thesis.

All data was integrated in ArcMap GIS (Global information System) software (Esri, 2012), where maps are generated. Coordinate systems were standardized to the World Geodetic System datum (WGS84) using the Universal Transverse Mercator (UTM) coordinates system projected for zone 34 north. All literature data used on this thesis has been georeferenced to this defined standard.
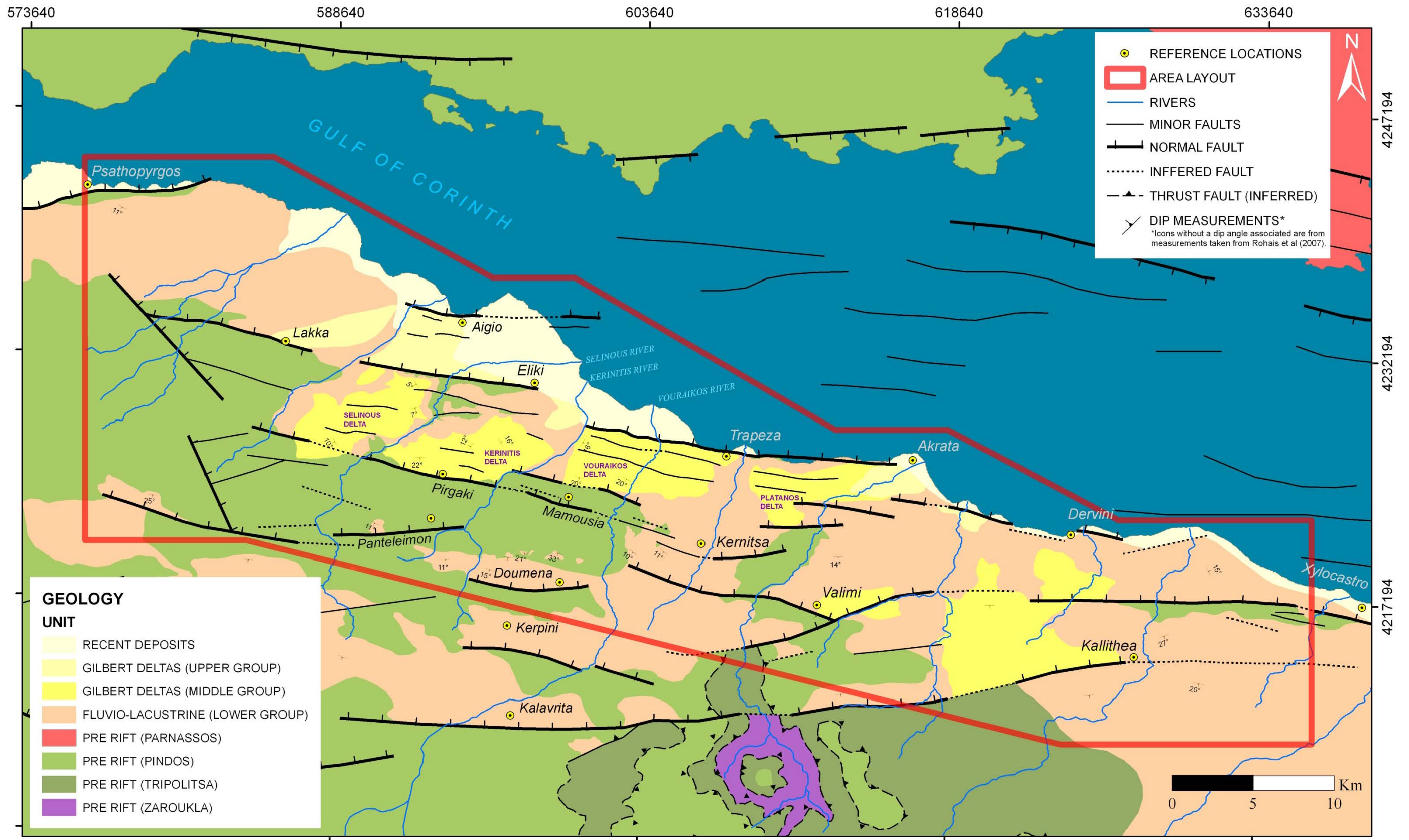
Figure 16 – Geological Map produced based on regional datasets (Figure 10, Figure 11, Figure 12 and Figure 13), field data (Figure 15), and the amalgamation and modification of key literature data (McNeill and Collier, 2004; Flotté et al., 2005; Ghisetti and Vezzani, 2005; McNeill et al., 2005; McNeill et al., 2007; Rettenmaier, 2007; Rohais et al., 2007; Benedicto et al., 2008; Ford et al., 2009; Backert et al., 2010; Leeder et al., 2012; Ford et al., 2013; Gobo, 2014b). Faults are shown mainly as independent segments and linkage of some key segments is discussed further on this thesis. Fault segment names derive form reference locations close to the fault trace. Plotted measurements are local trends and do not necessarily represent the regional trend of each unit, which will be discussed further on this thesis. Distinction between Upper and Middle group has been adopted from: (Ford et al., 2009; Backert et al., 2010; Gobo, 2014b). Basement unit (Pre-rift) variations are adopted from: (Benedicto et al., 2008; Papanikolaou, 2013; Hemelsdaël and Ford, 2015). The offshore extension of the Eghio Fault is derived from bathymetric data present by McNeill et al. (2007). Offshore faults are based on maps presented by: (Koukouvelas et al., 2001; Moretti et al., 2003)

Field measurements have been collected throughout the study area from both fault surfaces and bedding planes. These structural and sedimentary measurements are an important part of the field data, and have been plotted as poles of planes and lineament points on a Schmidt equal area lower hemisphere stereogram using the Open Stereo software. It is important to define that all measurements were acquired, treated and will be presented on a dip notation (dip direction/dip angle).

Plots were created and evaluated for each individual fault segment. These were integrated and analyzed as a group for each major fault zone, and finally a regional plot with the complete dataset was created to appraise the fault trend in the study area.

For sedimentary layers, stereograms for each location were statistically not significant. Therefore presented plots contain the complete dataset for either the Middle or the Lower Group.

Cylindrical best fits were calculated for each pole and point population and a representative measurement was derived by the adequate eigenvalue trend and plunge. These representative measurements aided regional interpretation and displacement estimation.

Displacements were calculated by projecting fault surfaces towards stratigraphic markers on hanging and footwalls. Because of different data constrains for each location, displacements for normal faults are classified as shown of Figure 17:

- Most Likely Displacement: when field data allows for control on fault surface and stratigraphic markers on the hanging wall and footwall;
- Minimum-Maximum Displacements: when unconformities are sub-cropping on hanging wall and/or are eroded from footwall. On such situations projections are made using representative measurements from the inferred closest topographical locations to where the unconformities could be and/or used to be exposed;
- Topography Derived Displacement: is approximated based on fault scarp controlled topography. This method uses the assumption that this fault scarp exposure is representative of the footwall uplift, and that the hanging wall drop is symmetrical and of the same greatness. This method was used in association with the previous two to provide a comparison value, and was used as a main values on faults where no constrains are available besides fault scarp topography.

MOST LIKELY

MINIMUM - MAXIMUM

UNEXPOSED UNCONFORMITY
AND UNCONSTRAINED
FAULTS ALLOW
FOR A MINIMUM
AND/OR MAXIMUM
ESTIMATE.

TOPOGRAPHY DERIVED

$$D = \sqrt{(X)^2 + (Y)^2} \qquad D = \frac{Y}{COS(90 - Fault\ Dip)}$$

$2 \times D \longrightarrow$ DISPLACEMENT

BASEMENT

FOOTWALL SEDIMENTS

HANGING WALL SEDIMENTS

FAULT

MINIMUM PROJECTIONS

UNCONFORMITIES
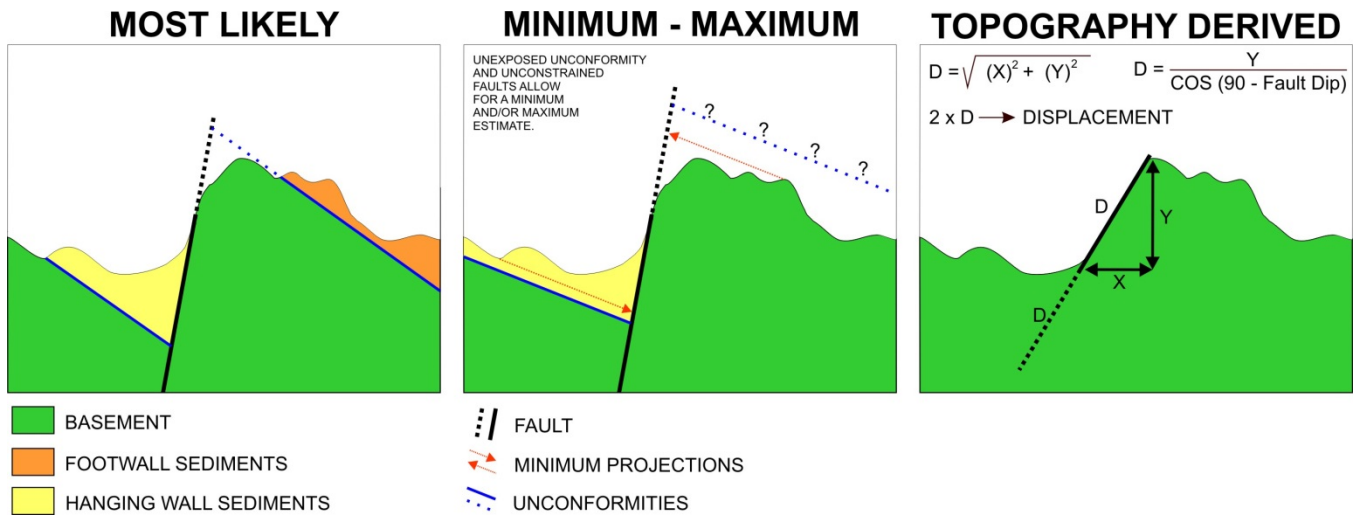
Figure 17 – Cross section sketch displaying how displacements were calculated and classified.

Displacements are calculated over cross sections that commonly are not parallel to dip directions of fault and/or stratigraphic markers. In these cases dip angles are adjusted to the appropriate apparent angles in the section before displacement estimates are calculated.

OBSERVATIONS

Geomorphology and Remote Sensor Compartmentalization

The geomorphological character of the Gulf of Corinth's southern coast clearly defines patterns on remote sensor datasets that are related to the structural and lithological field observations. Reflectance signature of different lithologies can be generally recognized, while regional lineaments are extracted from recurrent patterns on different products. Local lineaments are related to current river courses and topographic relief and also support structural compartmentalization and trends.

The remote sensor datasets show similar visual patterns on gravimetric, satellite compositions and DEM products. These regional patters can derive lineaments (Figure 18) that can help define a regional compartmentalization and large scale fault continuity interpretation.
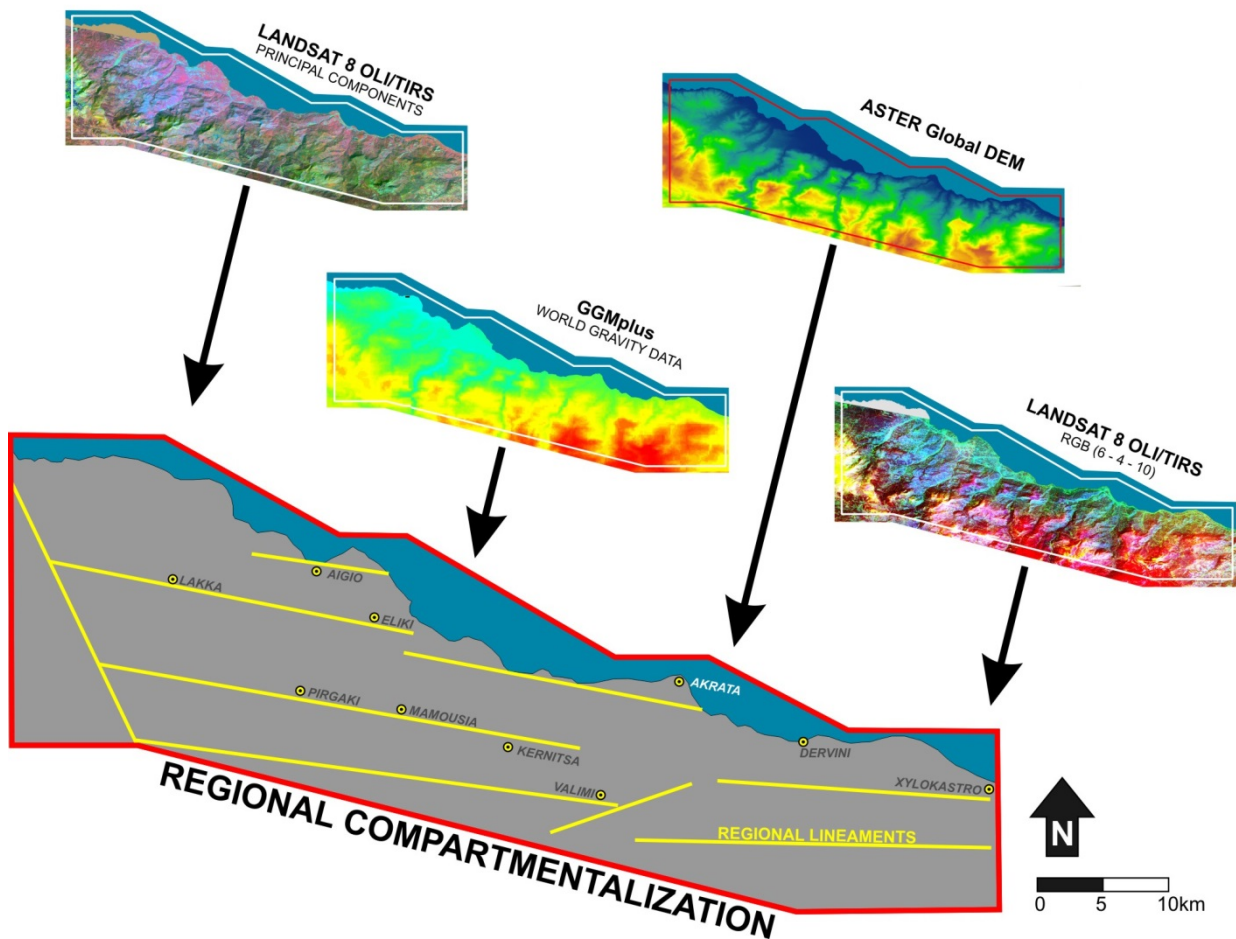
Figure 18 - Sketch of regional compartmentalization and lineament determination using the remote sensor products available.

Important observations from Figure 18 include:

- Regional lineaments up to 50 kilometers long are possible to be traced;
- The majority of lineaments are sub-parallel to the S75°E direction;

- Towards the west, a northwest to southeast lineament (sub-parallel to the S20°E direction) calls attention as it defies and truncate the regional lineament pattern;
- Regional lineaments cross over locations such as Aigio, Eliki, Pirgaki and Mamousia where important fault systems are known to exist.

Landsat 8 scenes (USGS, 2014) show a reflectance character correlation with field mapped lithology (Figure 15). This reflectance character does not show clear borders, but can be subdivided into at least four classes that are consistent with field lithological observations (Map of Figure 19). Generally, green dominant areas are related to carbonate basement, pink dominated areas are related to recent deposits and purple dominated areas are related to uplifted sediments from the Lower and Middle groups.
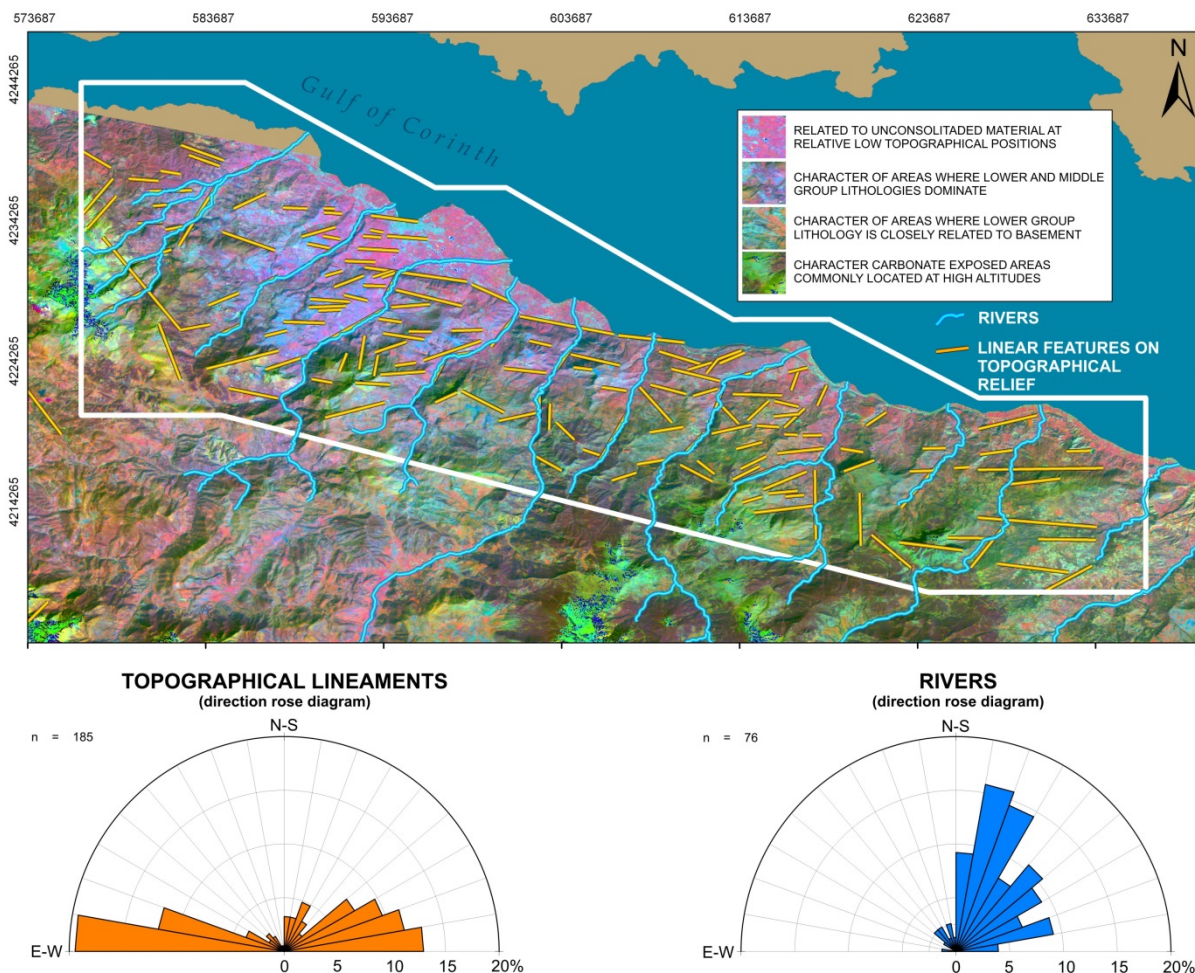
Figure 19 – Principal Component Landsat 8 RGB composition (Figure 11) (USGS, 2014), used for reflectance character correlation with lithology, and geomorphological lineament interpretations. Lineaments for both river course and topographical relief related are statically plotted on a rose diagram (180°) on Open Stereo software.

Regionally on remote sensor datasets, rivers can be generalized as sub-parallel lines on a north-south direction that are spaced reasonably evenly over the study area (Figure 19). When observed

on the field, it is not possible to generalize the river beds as straight lines without disregarding the topography. On field observation scale, rivers generally trend on a north-south direction by deflecting alternatively east and west.

Lineaments derived from aligned topographical relief have been interpreted using DEM and satellite composition datasets. Starting from a regional scale, lineaments are interpreted for the whole area. With a regional interpretation in hand, scale of observation was increased and the regional interpretation was consistently detailed. These lineaments are from 1 to 10 kilometers in length, with a mean of 2 kilometers. They show a predominant east-west direction with most traced lineaments varying between ± 15° from this general trend (Figure 20). Lineaments consistently match mapped fault locations (Figure 21) and regional lineaments (Figure 18).
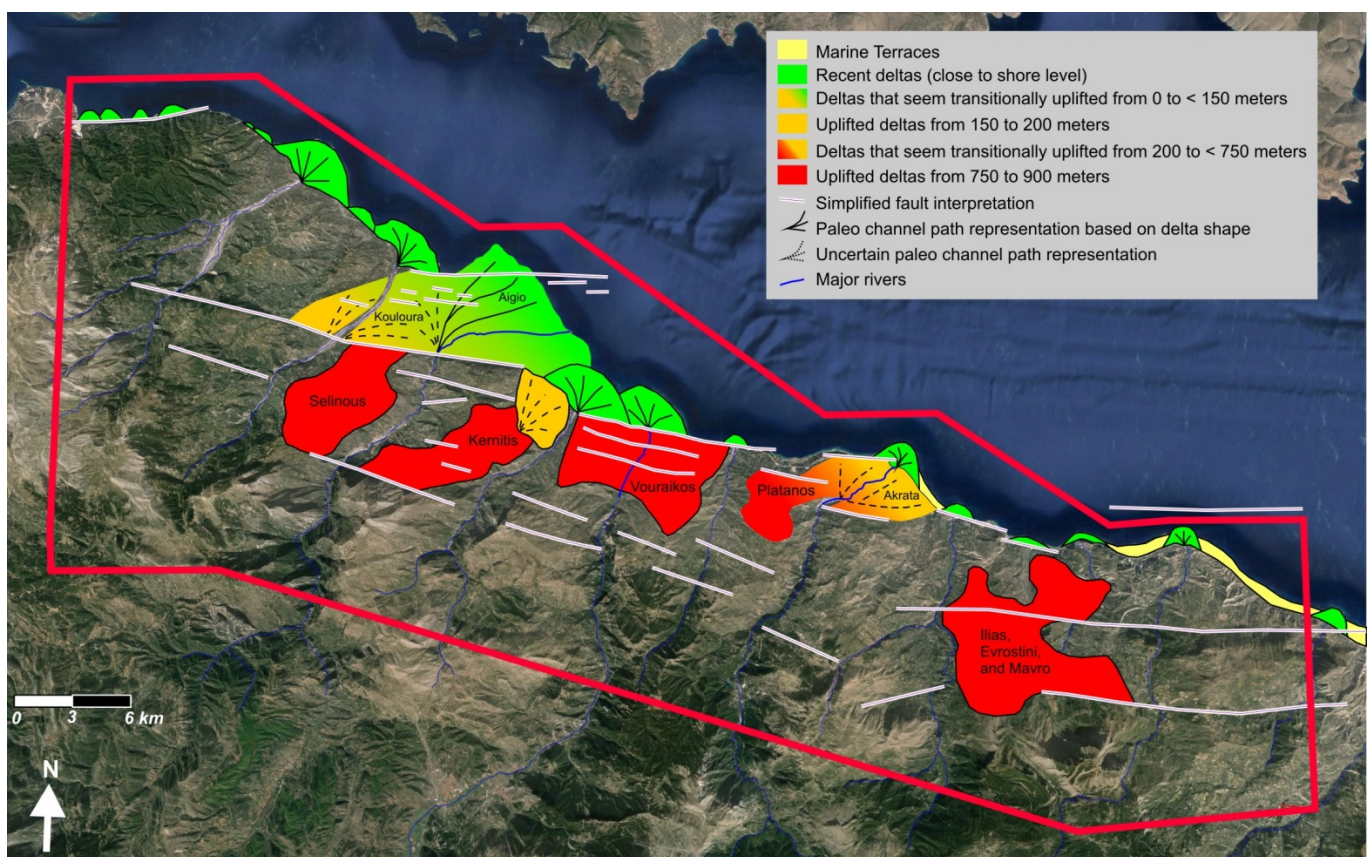
Figure 20 – Google Earth satellite image integrated with DEM showing delta units as defined by: (Ford et al., 2009; Backert et al., 2010; Gobo, 2014b). Delta units are highlighted and distinguished by topographical heights obtained from field observations and DEM datasets (USGS-METI, 2011).

By observing the delta units from the Upper and Middle groups in relation to satellite images and DMT models, other inferences can be made based on their relative altitude, elevation variability and transition (Figure 20).

The Upper Group recent deltas can be mainly defined as small to medium size, with characteristic symmetrical deltas shapes, and are abundant on the coastal area. These units occasionally overlap their edges and are located approximately at the current sea level (Figure 20). The Aigio Delta is distinctly different in size and shape to the other coastal deltas, with paleo channels that deflect towards the east and gradually increasing topography towards the southwest (2% slope). This gentle topographic slope allows for a smooth transition for the Aigio Delta with the Kouloura Delta that is 150 meters above the current sea level (Figure 20).

The Upper Group is also represented on Figure 20 as marine terraces that are mostly not observable on the western coast line and become visibly more extensive towards the east.

The Middle Group deltas do not retain any geomorphological shape resembling characteristic deltas, but are classified as deltas for the internal structures described on the literature (Ford et al., 2009; Backert et al., 2010; Gobo, 2014b). The modern rivers have eroded the Middle Group deltas so that most significant exposures are located between modern river courses. These exposures are located frequently at 750 to 900 meters above sea level, and present steep scarps defining their borders (Figure 28). From this, two exceptions are clearly notable:

- On the northern end of the Kerinitis Delta, an apparent radial shaped feature is distinctive. It presents a steep slope (22%) and is located between the steps of Eliki West with Eliki East Fault segments.
- At the northeastern end of the Platanos Delta, the Akrata Delta developed with a similar shape compared with the Aigio Delta. Although it presents a gentle slope of 4%, the Akrata Delta is entirely uplifted at least 60 meters above current sea level. This unit presents a modern river channel incising a valley that feeds a modern Upper Group delta at the coast line.

Structural

The main structural elements observable are related to faults. Although folds are frequently seen, they are restricted to basement lithologies and therefore were not described in detail.

Faults are commonly associated with a topographical expression on the form of elongated mountains and hills with steep slopes. Access roads between villages commonly transect the topography creating fresh exposures of fault planes. Fault exposures can also be reached by hiking or can be located high up on steep hill sides making them inaccessible for precise measurements. All fault planes observed, irrespective of their accessibility and contributions for stereograms are presented on Figure 21 and summarized on Table 1.
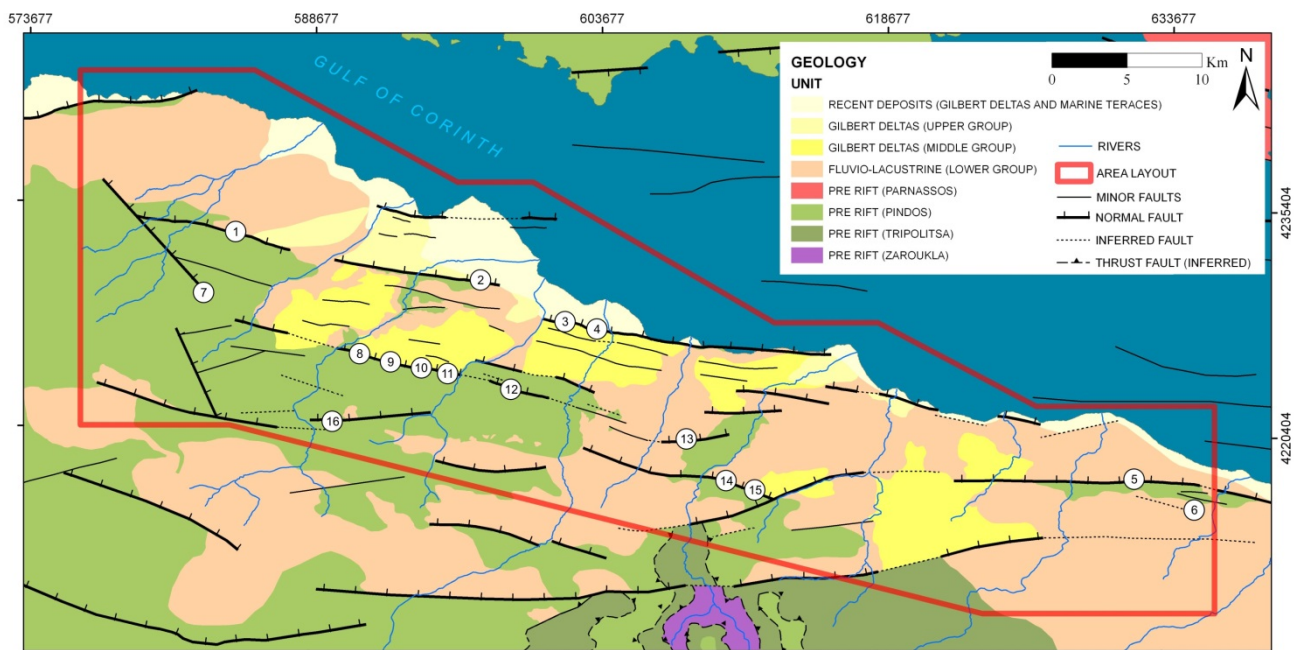
Figure 21 - Simplified geological map with fault plane locations numbered from 1 to 16. These locations are described in detail on Table 1. Due to the scale of the map, location 5 is composed of two outcrops; and location 6 is composed of three outcrops. Faults at locations 7, 9 and 16 were inaccessible and do not contribute with measurement data.

As can be observed on Figure 21, fault exposures tend to be distributed so that some northwest to southeast alignments are observable matching regional trends on Figure 18. Fault surfaces are non-continuously exposed along these alignments, as continuity is concealed by erosion and recent sediment covers.

Planes are commonly exposed on the scale of meters to hundreds of meters. They are rarely observed as flat planar structures on the field, but commonly are visible as gently curved along strike. This sinuosity of fault planes has been observed on a centimeter to hundred meter scale (Figure 22).

Table 1 – Summary of fault exposure locations with numbering pattern compatible with map shown on Figure 21. Coordinates are UTM projected for zone 34 north using the WGS84 datum. Altitude is obtained from the ASTER Global DEM (USGS-METI, 2011).

	FAULT	ALTITUDE	LATITUDE	LONGITUDE	FOOTWALL LITHOLOGY	EXPOSURE SCALE	Accessibility
①	Lakka	460	4232831	585846	BASEMENT	100 m	Hike
②	Eliki West	20	4230145	597796	BASEMENT	300 m	Road
③	Eliki East	60	4227109	603209	CONGLOMERATE	30 m	Road
④		40	4227514	601857	CONGLOMERATE	10 m	Road
⑤	Xylocastro North	450	4216131	635685	BASEMENT	50 m	Hike
⑤		350	4216256	635646	BASEMENT	15 m	-----
⑥	Xylocastro South	450	4216308	635259	BASEMENT	20 m	Road
⑥		250	4216743	635451	BASEMENT	5 m	Road
⑥		250	4217247	634914	BASEMENT	5 m	Road
⑦	Panachaikon	950	4230611	582230	BASEMENT	-----	Road
⑧	Pigarki	670	4224890	592233	BASEMENT	50 m	Hike
⑨		670	4224597	593061	BASEMENT	30 m	Hike
⑩		630	4224376	594932	BASEMENT	50 m	Hike
⑪		510	4224141	595910	BASEMENT	5 m	Road
⑫	Mamousia	850	4222849	599674	BASEMENT	10 m	Road
⑬	Kerinitsa	900	4220100	609995	BASEMENT	2 m	Road
⑭	Valimi	820	4217233	610374	BASEMENT	3 m	Road
⑮		870	4216971	610835	BASEMENT	5 m	Road
⑯	Panteleimon	1100	4220923	590366	BASEMENT	100 m	-----

At first glance, fault exposures seem like discrete structures, but with further observations these discrete exposures often are part of a damage zone. This is particularly clear for the Pirgaki, Xylokastro North and South segments, where damage zones range from 10 to 50 meters and are composed of a variable number of subparallel segments.

The Panachaikon segment was the most abnormal segment in the area, defined by an intensely fractured zone 10 meters wide, where fragmented basement rocks were associated with intensely striated calcite packages over a meter thick that contained angular rock fragments. No fault planes were clearly exposed, and the apparent direction this deformed zone is sub-parallel to the S20°E regional lineament direction (Figure 18) as represented on location 7 of Figure 21.

All fault locations were easily accessible, besides fault locations 9 and 10 on the Pirgaki segment that presented limited access, and location 16 on the Panteleimon segment were large exposures were mid slope and out of reach.

The footwall lithology in the region is predominantly the basement carbonates, while the Lower and Middle group conglomerates proved to be poor lithologies for exposing/preserving fault planes (Table 1).
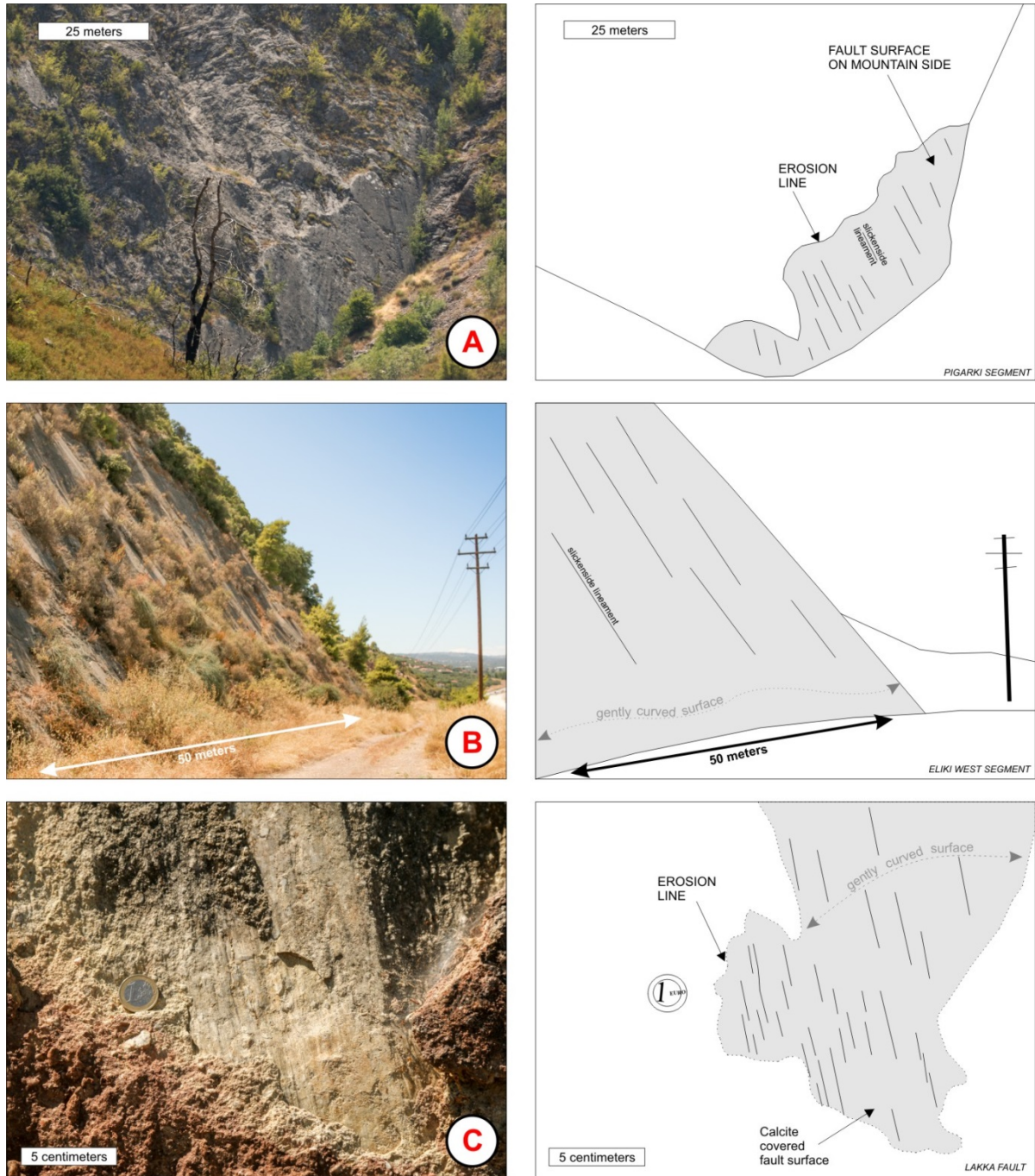
Figure 22 - Fault plane examples at different scales and over different lithologies. The set of pictures to the left are followed by a sketch of the observations on the right. All locations are defined on Figure 21 and on Table 1: (A) Pirgaki – Location 10; (B) Eliki West - Location 2; (C) Lakka - Location 1.

Fault planes were observed as smooth polished surfaces, often marked by parallel linear grooves called slickenside lineaments (Figure 22). On most occasions slickenside were engraved directly on the footwall lithology, but on the Lakka and Panachaikon segments a calcite layer covering the

36

footwall was engraved with the slickenside lineaments (Figure 22C).

Both fault plane and slickenside lineaments are plotted on Figure 23 and can be summarized on Table 2. Values are defined by the cylindrical best fit using all available data for each fault section.

Table 2 - Summary table of representative dip directions and angles derived from the stereograms of Figure 23 for slickensides (lines) and fault surfaces (planes). Additional information such as data point density and footwall lithology is available.

	SLIKENSIDES			LINE DATA POINTS	SURFACE (PLANE)			PLANE DATA POINTS	FOOTWALL LITHOLOGY
	DIP DIRECTION	/	DIP ANGLE		DIP DIRECTION	/	DIP ANGLE		
LAKKA	341	/	41°	5	031	/	51°	10	CARBONATE
ELIKI WEST	020	/	56°	12	012	/	54°	29	CARBONATE
ELIKI EAST	--	--	--	0	010	/	59°	14	CONGLOMERATE
XYLOCASTRO-N	015	/	68°	6	355	/	70°	25	CARBONATE
XYLOCASTRO-S	340	/	40°	9	024	/	56°	64	CARBONATE
PIRGAKI	017	/	61°	38	012	/	59°	57	CARBONATE
MAMOUSIA	045	/	68°	7	030	/	69°	32	CARBONATE
KERINITSA	024	/	62°	6	335	/	69°	25	CARBONATE
VALIMI	--	--	--	0	028	/	56°	28	CARBONATE
ALL FAULTS	**015**	**/**	**68**	**88**	**018**	**/**	**56**	**302**	-----

Fault planes are represented on stereograms as poles of planes and are symbolized by red contour areas (Figure 23).

Slickenside lineaments are plotted as lower hemisphere line interception points and their distribution is represented by blue contour areas (Figure 23).
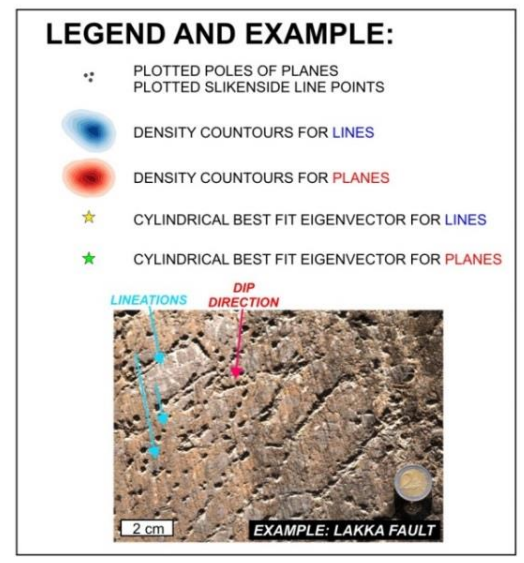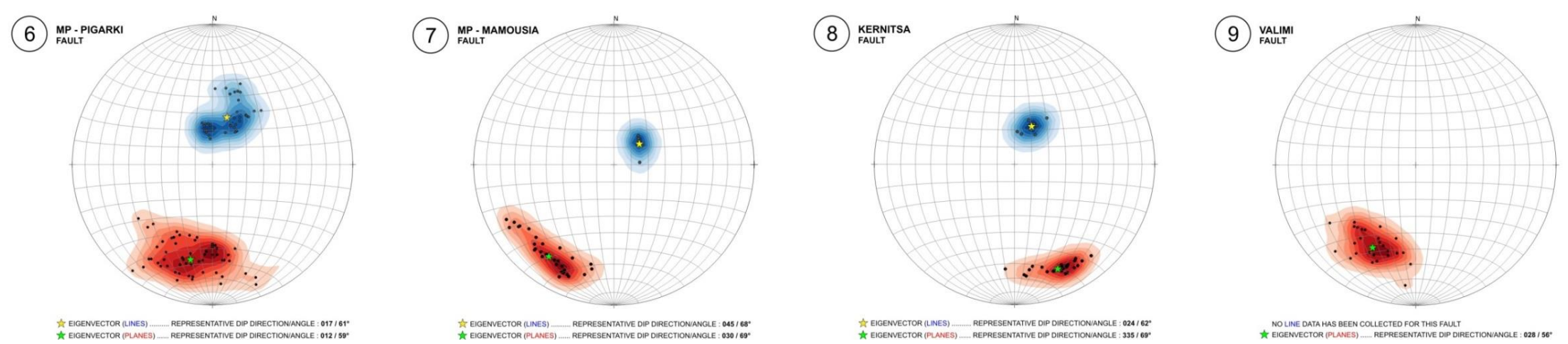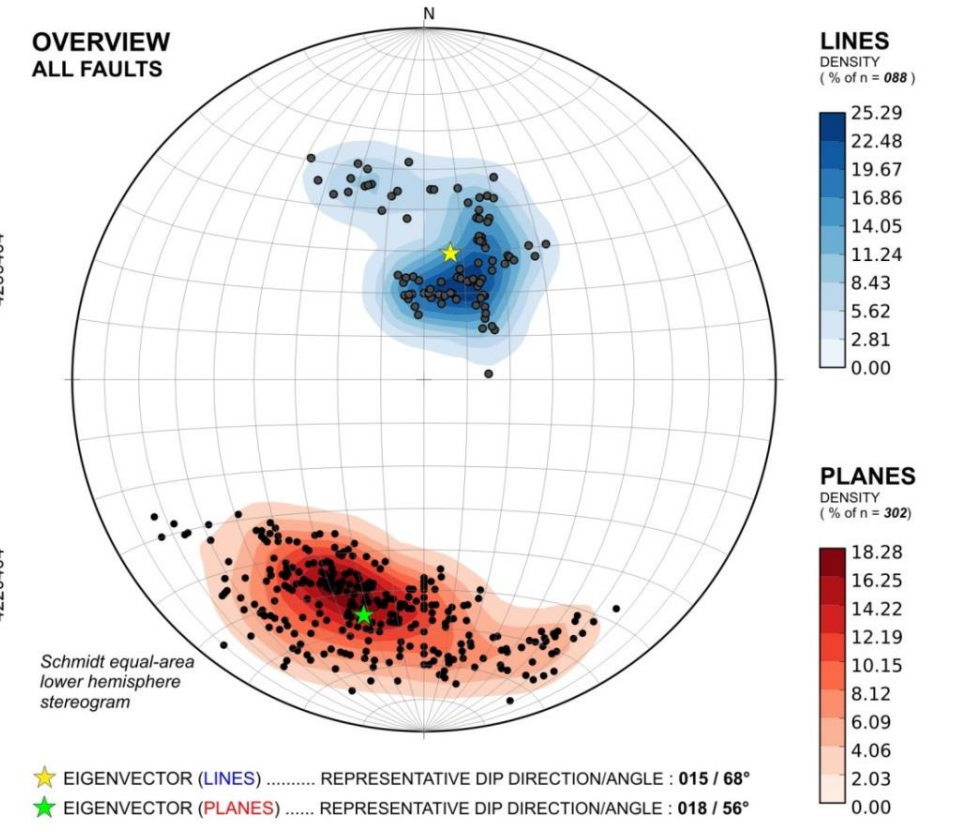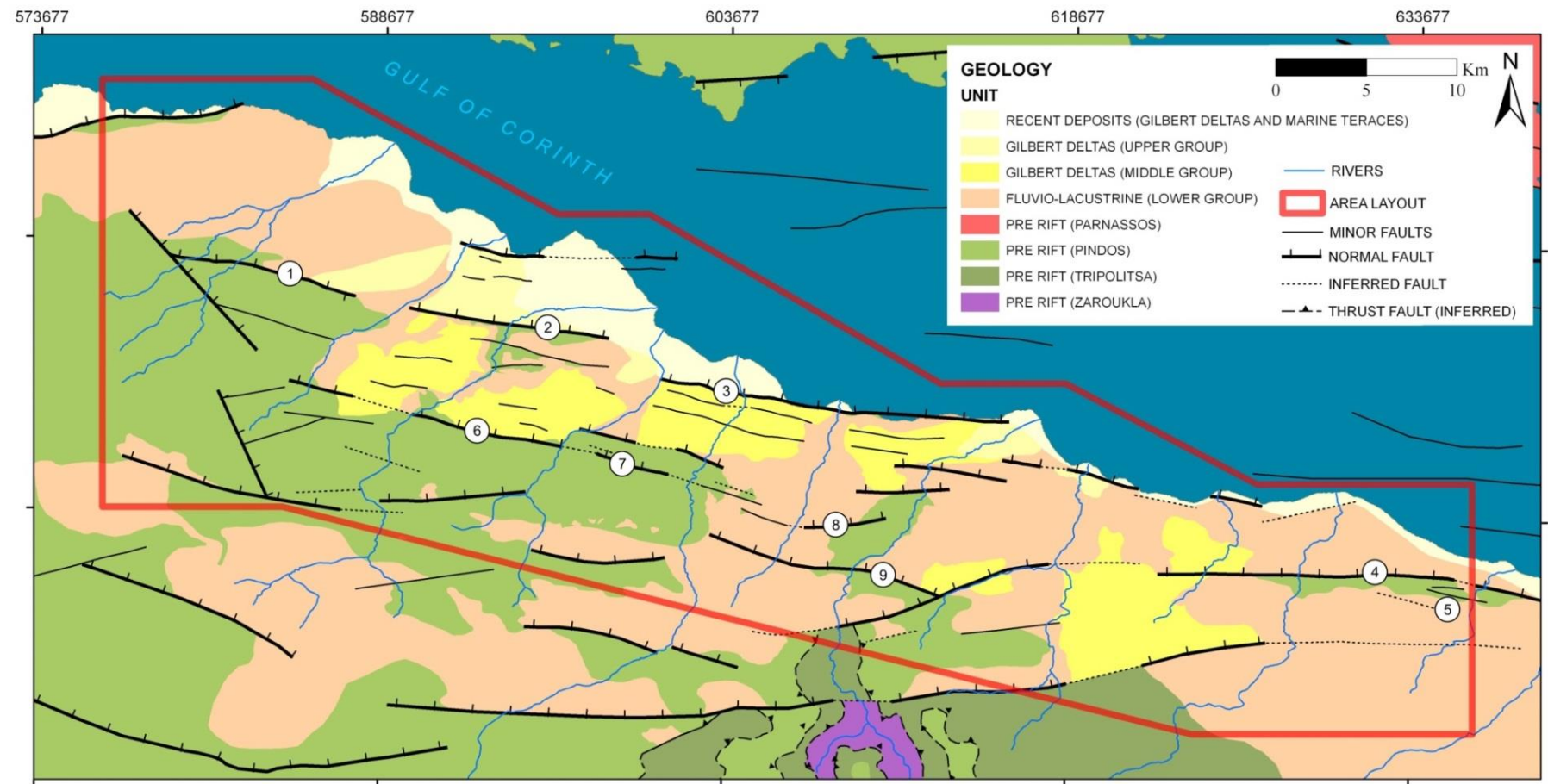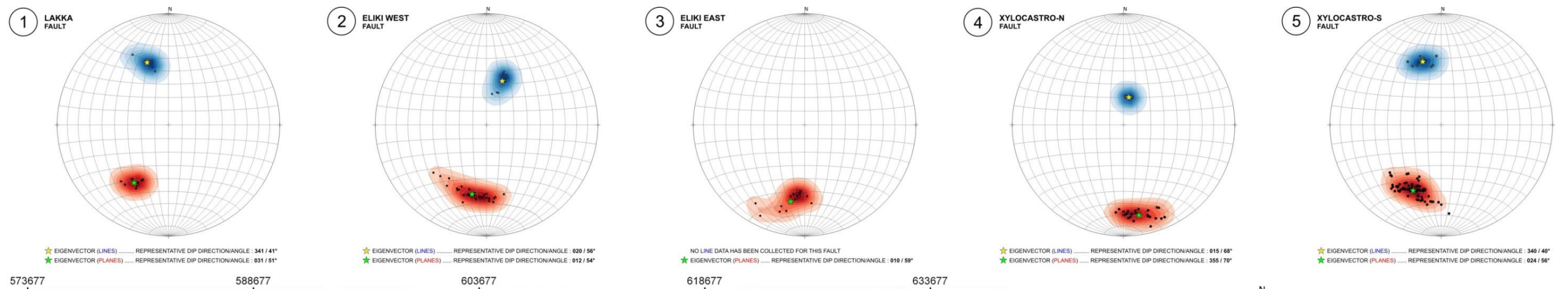
Figure 23 - Schmidt equal area lower hemisphere stereogram overview for structural elements: fault surfaces (PLANES) and slickenside lineation's (LINES). All measurements were taken on a dip direction notation (Dip Direction/Dip Angle) and are plotted as poles of planes (red contours) and line points (blue contours). All measured faults are labeled, numbered and orientated on the simplified map. On the right corner a representative picture of a fault surface and slickenside lineation's is displayed. Plots 2, 3 and 6 were populated with measurements from the same fault on different locations that were well distributed along the fault line, and therefore the data is more representative of the fault as a whole. Plots 4, 5 and 9 were populated with measurements from the same fault on different locations, but these were close apart and have less significant representativeness over the fault segment as a whole. Plots 1, 7 were populated with measurements of well exposed fault planes on a single outcrop and therefore have the least representativeness of the fault as a whole.

38

Individual and regional overview stereograms from Figure 23 indicate that faults on the region have dip direction varying continuously between N36°W to N60°E. For the overview plot, the best fit plane matches closely with the high density contour area at N18°E.

Regional dip angles vary from 40 to 80°. From the plots on Figure 23 it is hard to distinguish a clear pattern of increase or decrease on an east-west or north-south direction. Plots 6 and 9 show the higher dip angle variability for an individual segment reaching up to 30° range. For the overview plot, the best fit plane is close to the high density contour area at 56° dip angle.

Not all fault surfaces presented measurable lineaments and therefore blue contours are missing for plots 3 and 9. Plots 2, 4, 6 and 7 present slickenside lineaments that are sub-parallel to the dip angle and direction of the planes they imprint, while plots 1, 5 and 8 show lineaments clearly dipping obliquely related to the dip direction of their fault plane. This obliqueness is in the order of 10 to 35° from plane dip direction. These oblique dipping slickensides were clearly observed on an outcrop scale and are sketched on the right corner representative picture shown on Figure 23.

Slickenside lineation's frequently present a distinctly more concentrated distribution spread compared to their counterpart fault planes. Often lineations are concentrated on a direction, while fault planes show reasonable direction variability. This fact has been observed on field and has been consistently proven even when lineament sampling was carefully done over different representative fault plane directions on a single outcrop.

Lithological

Although all the syn-rift sediments described on the literature were observed on the study area, only the Lower and Middle groups will be described in detail. The basement rocks are considered an undifferentiated unit and observations were limited, and the Upper Group unit is non-lithified and mostly unexposed, being classified mostly by its geomorphology.

Field observations have shown that the basement is predominantly formed by carbonates that are deformed with a complex folding patterns and small offset faults. Tight symmetric and asymmetric folds, with or without vergence are common on observable scales of centimeters to tens of meters. Exposed flanks of anticlinal or synclinal folds also show slickenside lineaments on sub perpendicular angles to the fold hinge. These surfaces and lineaments could lead to confusion related to regional steep dipping fault planes, and therefore outcrops were occasionally inspected in detail.

Other less dominant basement lithologies were observed and identified as marls, cemented breccia's, fine grained sandstones with carbonate cement, phyllites and chert lenses.

Basement exposures are often found from deep valleys to high mountain ridges. Small isolated outcrops are also mapped in gulleys located in the middle of sediment dominated areas, and are illustrated by small green markers on Figure 24.
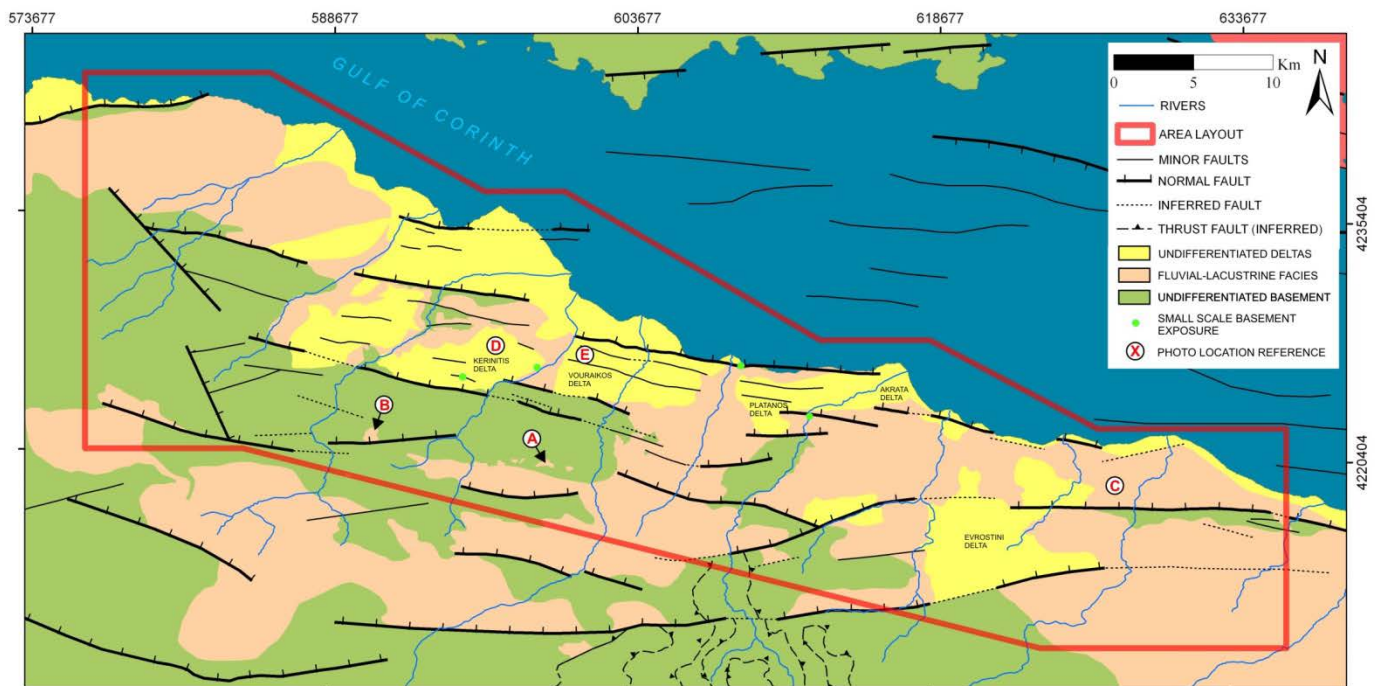
Figure 24 - Simplified geological map with locations of outcrops labeled as A, B. C. D and E. Locations are also shown on Figure 25 and Figure 26. Small scale basement outcrop locations are also highlighted by green markers across the map.

The unconformity between the basement and the overlying sediments was visible only behind the Mamousia segment and can be classified as an irregular surface (Figure 24A and Figure 25A). On all other locations the unconformity was mapped with aid of remote sensor datasets together with field observations related to change of lithology between outcrop locations.
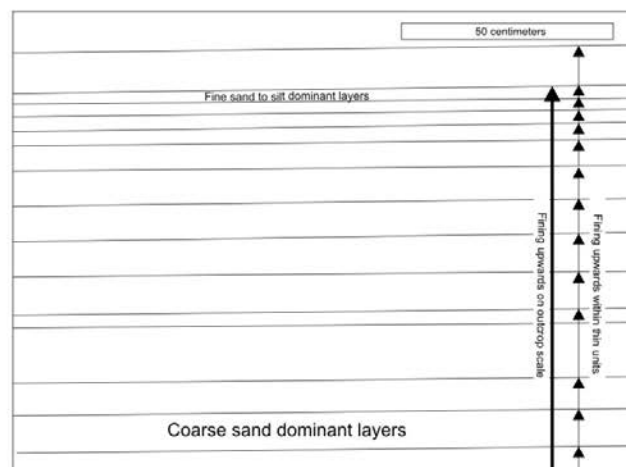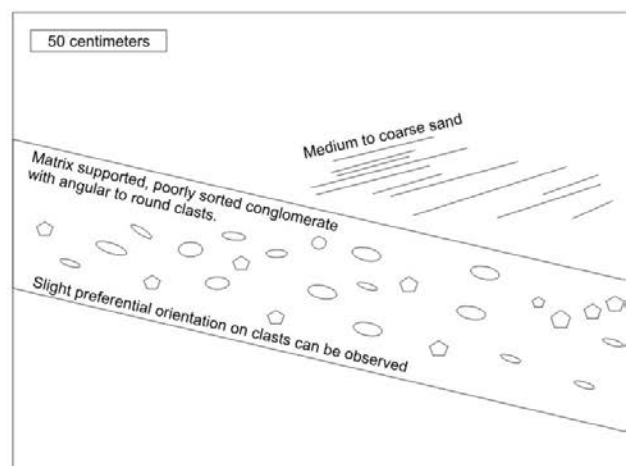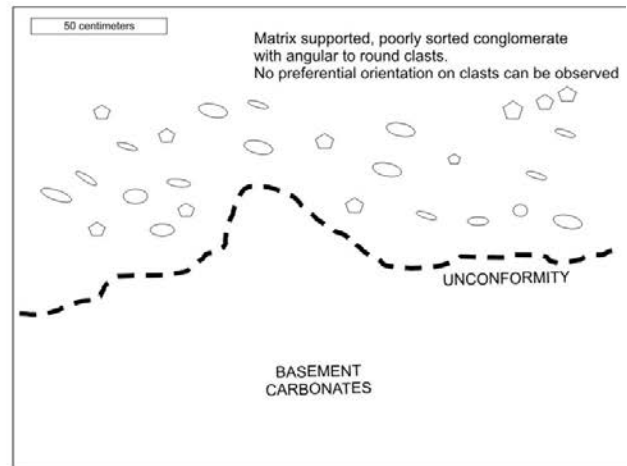
Figure 25 - Lower Group outcrop examples. (A) basement-conglomerate contact over an unconformity; (B) conglomerate with occasional sand units predominant on the south; (C) parallel bedded sand and silt unit dominant on the north. Outcrop locations are shown on Figure 24.

The Lower Group was observed to be a widespread unit that outcrops locally over most of the extent of the study area (Figure 24).

Towards the south this unit is characterized predominantly by a lithified matrix supported conglomerate with occasional sand prone units that erode and/or onlap the coarser unit (Figure 25B). The conglomerate is built of poorly sorted clasts that vary from angular to round. These clasts are composed mainly of carbonate and chert with size ranging up to 40 centimeters. Orientation is poorly expressed and no attempt was made to collect flow direction data.

Parallel bedded sand and silt dominant units are prevailing on northern outcrops towards the coast line (Figure 25C). These were observed with up to 250 meters of successions showing a clear pattern of fining upwards, visible both on an individual bed (centimeter) and outcrop scale (3 meters).
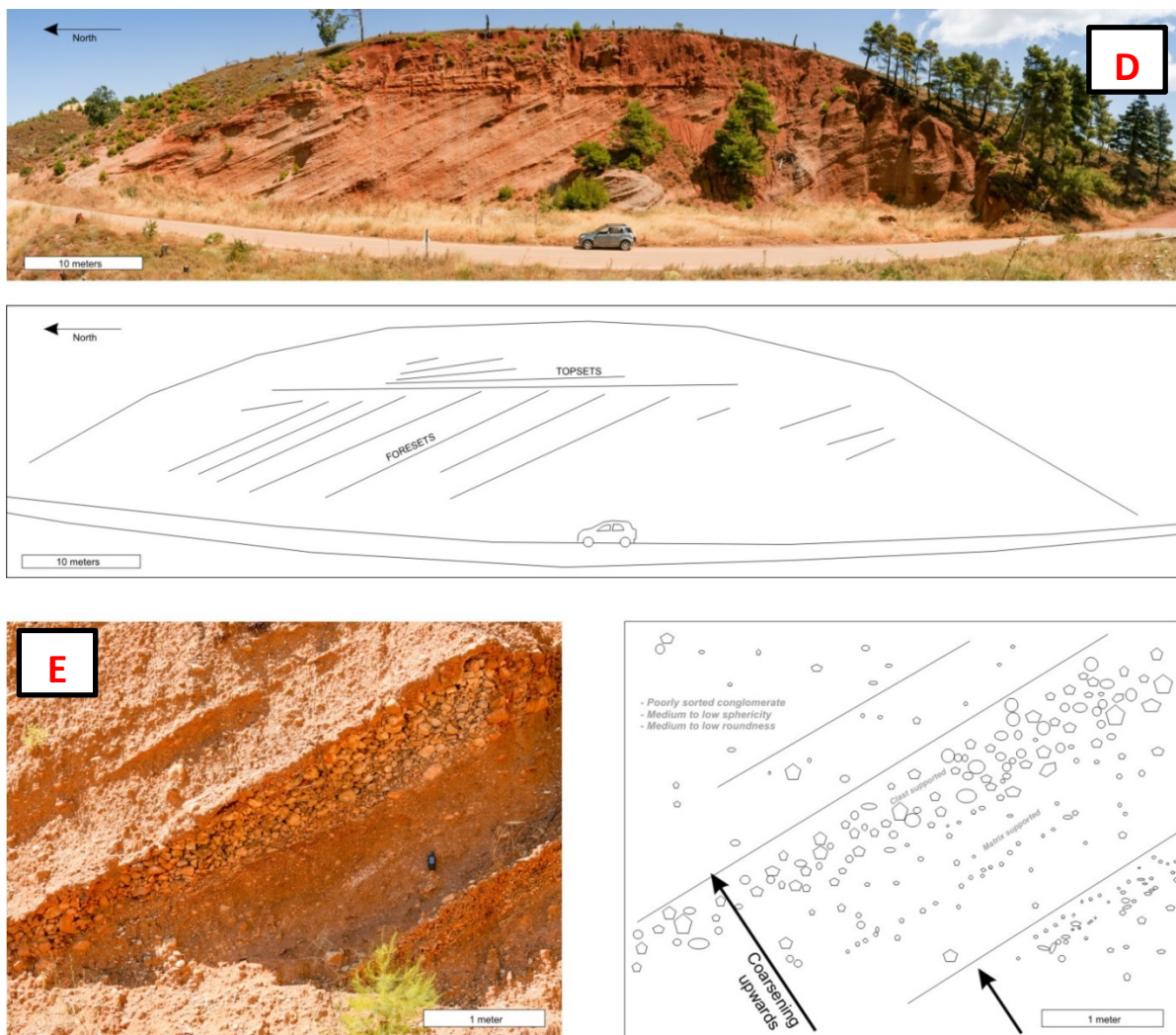
Figure 26 – Middle Group conglomerates exposed on high topographical elevations, with topsets, and foresets clearly visible indicating a northward flow direction with a coarsening upward sequence clearly identified. Outcrop locations are shown on Figure 24.

Delta units can be subdivided into a group of coastal depositional systems that are active today and are mainly present on sea level with limited exposures (Upper Group), and an exposed group that is up to 850 meters above sea level (Middle Group) (Figure 26).

The Middle Group is exposed mostly behind the coastal fault system composed of the Eliki East and Eliki West segments, extending to the Mamousia-Pirgaki Fault system to the south. This group can be described as a gravelly unit characterized predominantly by conglomerates that vary from matrix supported to clast supported (Figure 26E). Clasts are poorly sorted and vary from angular to round, composed mainly by carbonate, marl, chert and other conglomerate fragments, most of which are up to 20 centimeters in size. A coarsening upward sequence can be defined within the unit and a general orientation is defined by topset and foreset relation which indicates a predominant flow towards the north (Figure 26D). This unit is observable on road side exposed profiles that uncover a continuous succession of up to 450 meters.

Both Middle and Lower group unit beddings were plotted on stereograms on Figure 27. Measurements related to the Middle Group were carefully divided into topset and foreset, while only topset distributions were statistically relevant.
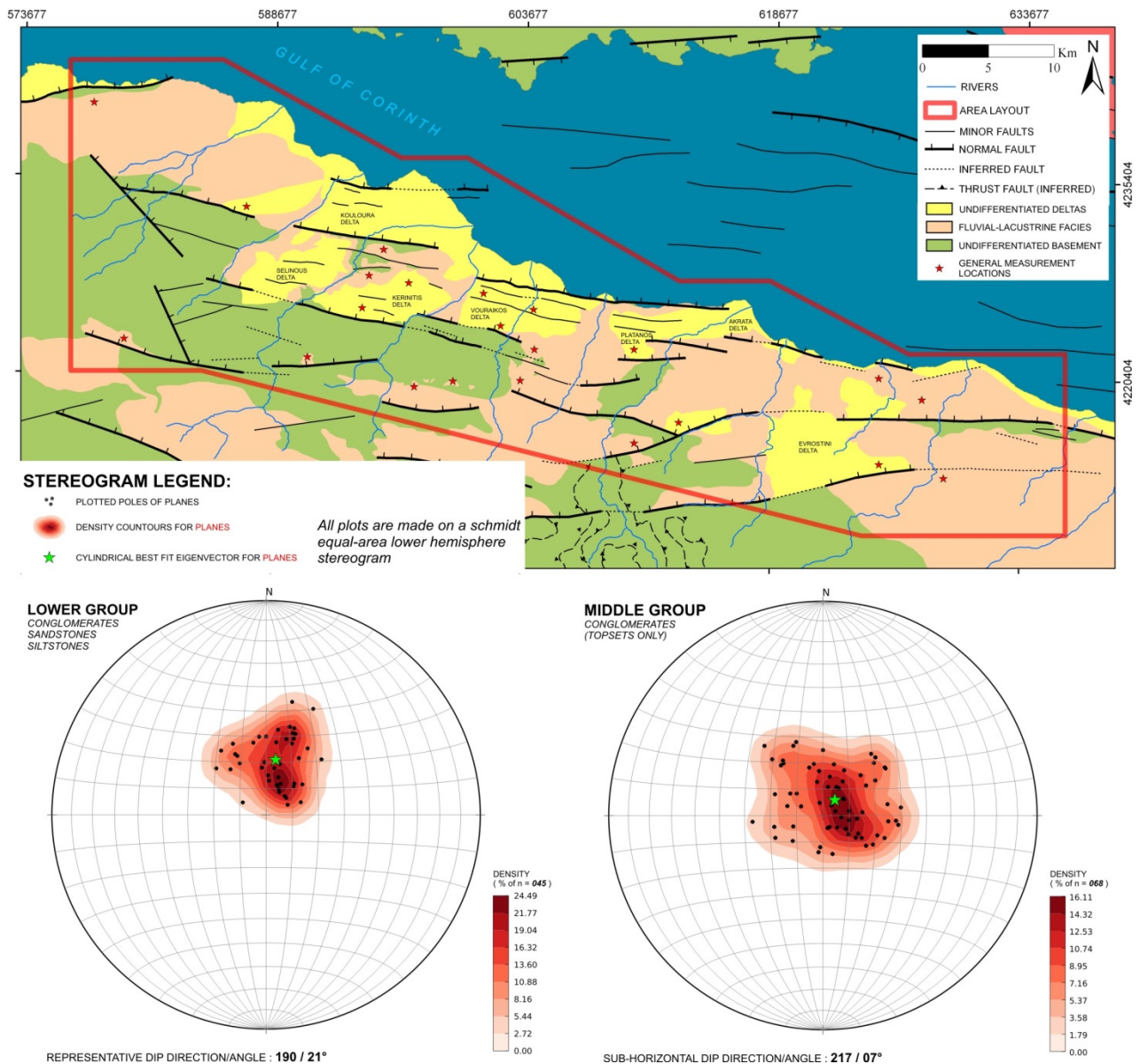
Figure 27 - Schmidt equal area lower hemisphere stereogram overview for Lower and Middle group regional layer dip direction and angles, associated with representative geological map displaying main sampled locations. Middle group plotted values are associated only to topsets.

Although dip measurements are spread over an extensive area and were collected over the rugged surface of conglomerate beddings, the stereograms on Figure 27 show a reasonably ordered pole distribution with a low spread.

The Lower Group has an approximate 20° spread around the best fit and high density location. The regional representative dip direction is S10°W with all points of this group consistently dipping on directions between S20°E and S25°W. The representative regional dip angle for this unit is 21°.

For the Middle Group the range is slightly larger than the one described for the Lower Group with a

30° spread around the best fit location. The regional topset dip angle is 7°, and because of its sub horizontal character associated with measurement errors, it is important to highlight that this value by itself may not be representative. Although the absolute value may not be descriptive of the whole group, the pole cloud distribution shows a slight southern dip trend.

Panorama on Figure 28 shows an approximate 400 meters succession of topsets and foreset (Middle Group). From this representative photo a similar relation is observed when compared with the pole cloud distribution shown on Figure 27, with topsets mostly dipping southwards and few distal portions slightly dipping northward. It is important to note that most observed dips are probably apparent dips (not observed on a perpendicular profile related to the surface dip direction). Nevertheless the section is approximately north-south orientated and the apparent dips should be approximately the same as real dips.
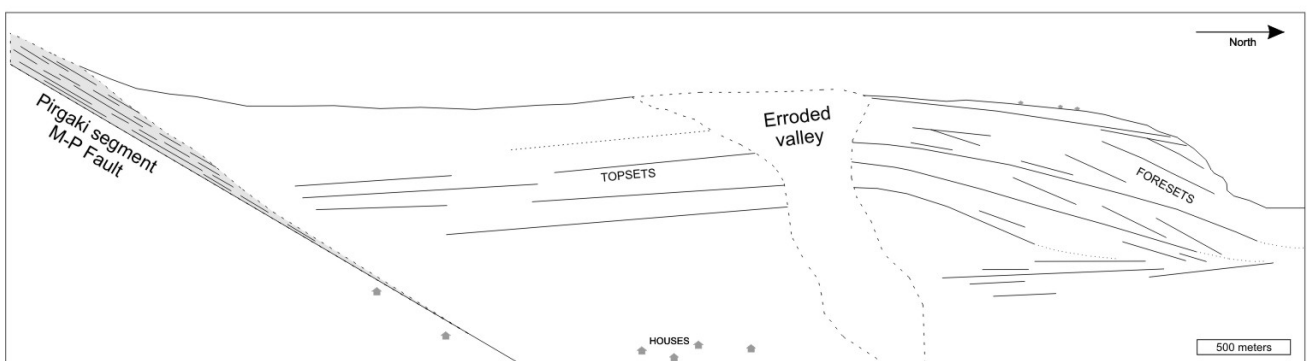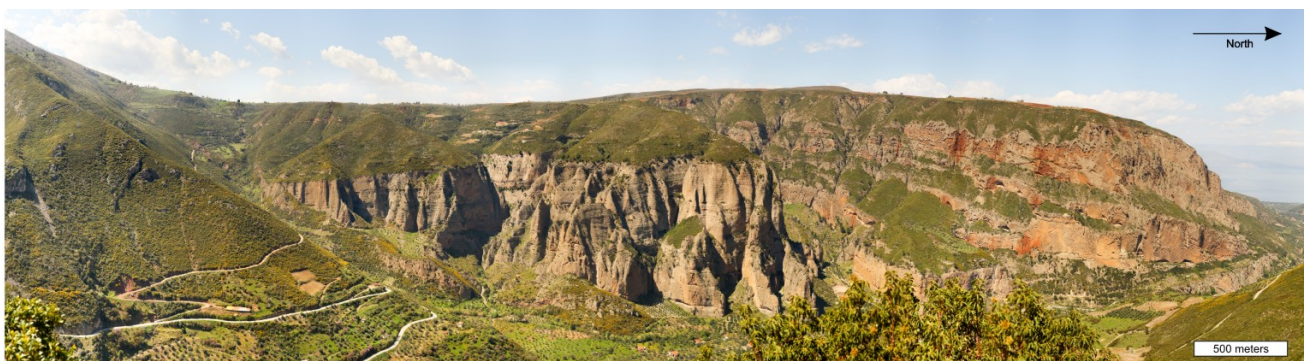
Figure 28- Giant deltas (Middle Group) in relation to Pirgaki segment of the M-P Fault with topset and foreset observations highlighted. Panorama was produced with equirectangular projection so that lines on the center of the picture are minimally deformed, and the distorted area of the picture was cropped.

The Pirgaki segment of the Mamousia-Pirgaki Fault is sketched on the image on areas where fault planes have been found (Figure 27). The direct contact of the delta with the fault surface is covered by recent sediments flowing down the mountain side, but topsets seem to be approaching each other as they close into the fault surface.

INTERPRETATIONS AND DISCUSSIONS

Field observations are aligned with regional datasets and literature data to produce interpretations of the southern coast of the Gulf of Corinth within the presented study area. The means of which these three sources of information align may produce discussions and ambiguities, and whenever information available is not enough, multiple options will be presented and discussed.

The arrangement of this chapter is defined by an initial structural discussion that develops to embrace sedimentological interpretations. With these concluded displacement estimates will be presented associated with geological profiles.

Although, major faults are frequently drawn on maps and discussed as if they were discrete structures that accommodate large displacements, key literature data derived from studies using core and trench data have described faults in the region as fault zones (Figure 29) (Koukouvelas et al., 2001; Micarelli et al., 2003; Pavlides et al., 2003). Fault zones are supported by field observations on the Pirgaki and the Xylokastro segments where a zone approximately 50 meters wide is present containing multiple subparallel fault surfaces. Few extensive discrete fault surfaces have been observed (e.g. Lakka, Eliki West and East segments), but fault zones may still exist at these locations with erosion, soil and sediment covers playing an important role on what is visible or not.

From the detailed profiles shown on Figure 29 and field observations, fault zones are composed of several faults that dip at different angles towards the same general direction. This dip angle variability has been observed on stereograms of Figure 23, and can be explained both by dip variability within a single discrete fault surface and/or by separate discrete structures that compose the same fault zone and dip at different angles (Figure 29).

Based on observations, major faults in the region can be classified as composed of fault zones that are up to 100 meters wide. These zones can contain discrete surfaces that are laterally extensive while the fault zone can be unexposed. Deformation within the zone takes place mainly as faults, with folds being rarely visible and hard to distinguish from pre-rift basement deformation.
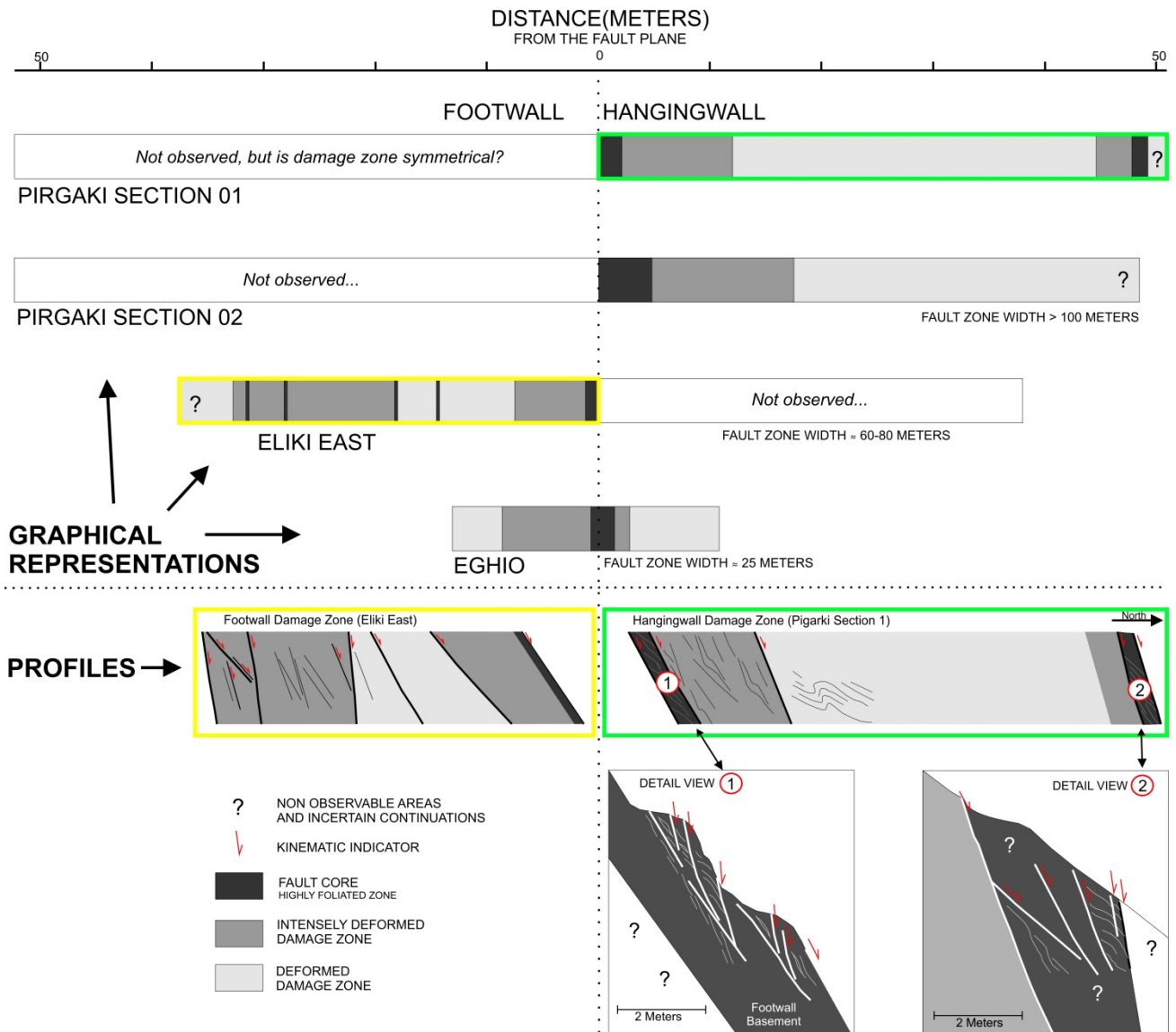
Figure 29 –Graphical characterization of major fault zones in the study area modified from: (Koukouvelas et al., 2001; Micarelli et al., 2003; Pavlides et al., 2003). Field data has been integrated on Pirgaki Section 02. From top to bottom: (i) Four graphical representations of damage zone within footwall and/or hanging wall of major fault in the region (ii) Two profile sections with color coded borders showing respectively from left to right the footwall damage zone for Eliki East and the hanging wall damage zone for Pirgaki; (iii) Two profiles with detail views of the cores of the Pirgaki hanging wall damage zone and structures within.

Slickenside lineaments are commonly used as kinematic indicators and interpreting these striations may provide important information about faults in the region:

- Slickenside visible over calcite recrystallization on fault surfaces (Figure 22C) indicates possible fault surface reactivation.
- Striation patterns in relation to fault dip direction (Figure 23) suggest that oblique slip is present on some faults in the region.

The oblique slip indicators could result from change of fault orientation or by oblique normal faulting. As fault segments are mostly mapped as sub-linear features, oblique normal faulting is a

48

likely suggestion. With oblique faulting considered, displacement can be divided into a down-dip and a strike-slip component. The strike-slip component is likely to generate a tip damage zone that is accompanied by a variety of possible structures, among them horsetail splays, branched fractures or wing cracks as shown on Figure 30 (Kim and Sanderson, 2005). These fault tip structures, if present, can provide an explanation for current geomorphological patterns and fault linkage over stepping segments (Figure 30 - Examples)

It is important to notice that fault tips have not been observed in the field, and consequently all the related structures illustrated on Figure 30 are only a theoretical possibility. It is also significant to highlight that the scale of this project is not adequate for detailed structure mapping. Therefore, although these structures have not been mapped, they should not be entirely dismissed.
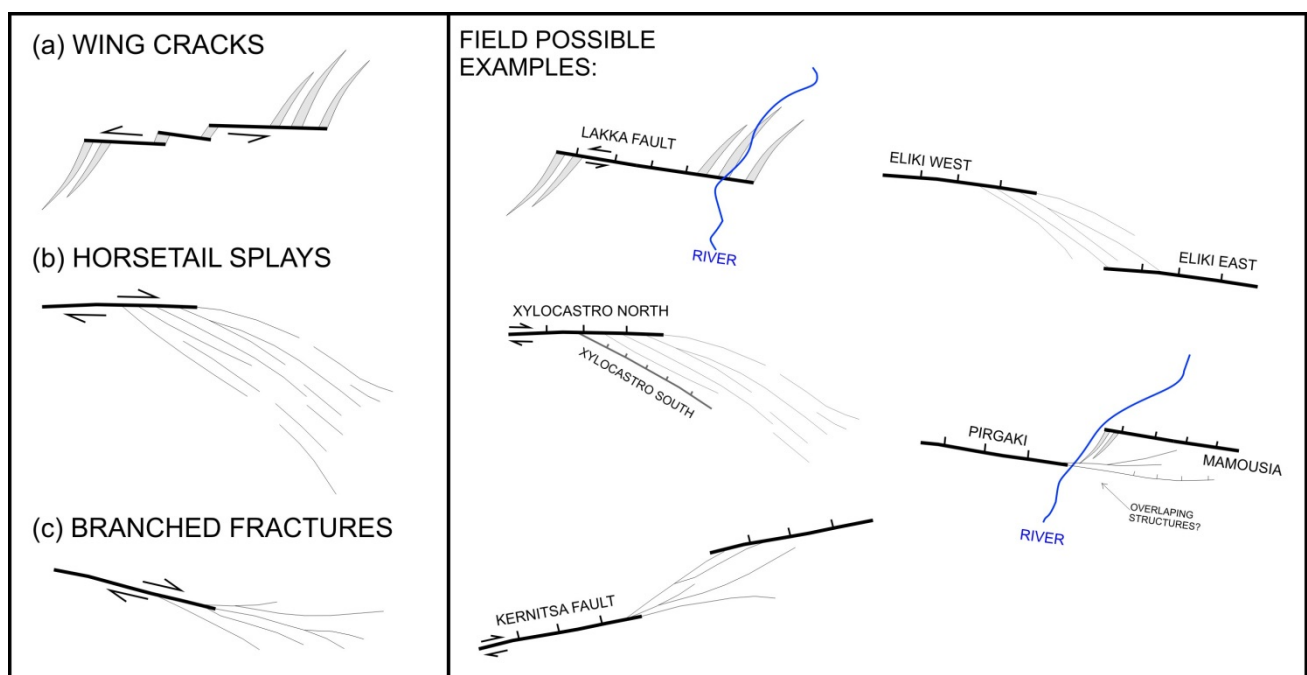
Figure 30 - Fault tip structures modified from Kim and Sanderson (2005) and adapted to Gulf of Corinth fault situations.

The linkage between fault segments is an important topic in the study area, and although more than one possibility exists, the locations where segments would link are frequently not exposed and observations are indirect and limited.

The major fault segments are frequently not aligned and connected over steep eroded valleys that cut sub-perpendicularly to the fault strike direction (Figure 16). Topographic relief is usually high on both valley sides suggesting that fault segments do not tip on the valley itself, but that these fault segments are rather linked (Figure 2).
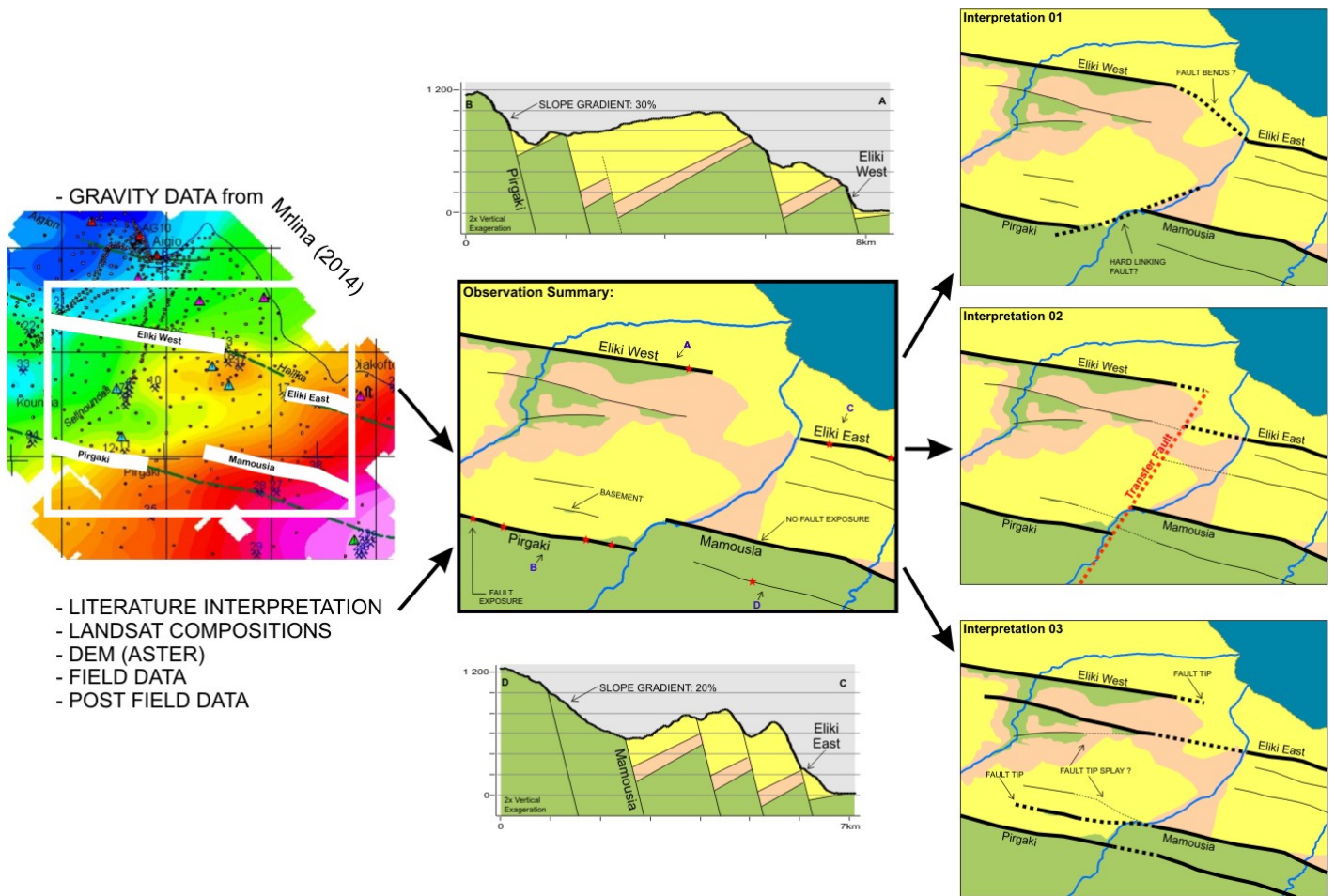
Figure 31 - Sketch to discuss fault step interpretations. Three proposals are done (right images) base on the central summary map and geological profiles associated. All remote sensor data presented have been used to aid interpretation proposals.

The major north dipping fault zones are commonly interpreted on the literature and observed in the field as being composed of two to more non-aligned segments. Two major examples are the right stepping Eliki Fault segments, and the left stepping Mamousia-Pirgaki Fault segments (Figure 31). Commonly these segment connections have not been discussed in detail, but using field data together with remote sensor datasets, three possible interpretations will be considered:

1. Few authors have provided their opinion over fault linkage in the form of maps, and these interpretations are exemplified on Figure 31 – Interpretation 1 (Benedicto et al., 2008; Ford et al., 2013):

    a. The Eliki segments bend at their tips until they connect;

    b. The Pirgaki and Mamousia segments show a hard link (fault or breached relay ramp).

Even though a relatively tight bend between the Eliki segments is unexpected on a region where lineaments are mostly straight (Figure 19), topography shows an inflection in the area

50

supporting the bend interpretation (Figure 20). Theoretical fault tip structures such as horsetail splays could aid the fault linkage mechanism as shown on the sketch of Figure 30. Still, the lack of clear field observation is a weak point of this interpretation.

The Mamousia-Pirgaki hard link is also a possibility and could be aided by the theoretical fault tip structures such as wing-cracks (Figure 30). Heavy erosional process and the Middle Group covers are a big challenge for observations.

Both explanations for fault step do not clarify if and how minor faults are linked, and particularly for the Mamousia-Pirgaki segment, it creates an extra difficulty on explaining the basement exposure that is in front of the Pirgaki segment on a high topographical position (750 meters above sea level) (Figure 31).

2. Interpretation 2 (Figure 31) is supported by Mrlina (2014) who maintains that lateral variations on Bouguer corrected gravity data (Figure 13 and Figure 31) is an indicator that transfer faults divide laterally the Eliki West and Pirgaki segments from the Eliki East and Mamousia. To address this interpretation, the following three points should be evaluated:

   A. Literature on transfer faults (Etheridge, 1986; McClay and Khalil, 1998; Acocella et al., 2005) indicate that these structures are not usually described on continental narrow rift settings. Acocella et al. (2005) using sandbox experimental data associated with a qualitative comparison with analogs suggests that transfer faults need significant stretching to develop, and therefore are far more common on passive margins, back arc basins and wide rifts (e.g. Basin and Range, North Sea and Mojave Desert). The same author suggests that transfer zones are predominant on narrow rifts (e.g. Rio Grande, Rhine graben, East African Rift System and Baikal).

   B. Pre-existing faults and weaknesses on the basement are a possibility that can be considered. These weaknesses would be an important factor on the development of transfer faults. As no consistent observation of the basement has been done, regional preferential weakness directions cannot be deduced.

   C. Considering transfer faults exist, they would closely coincide with river incised valleys that have an apparent linear direction on a regional view (Figure 19 and Figure 31). As has been

observed previously, these river valleys are not linear on smaller observation scales. From this observation two lines of discussion are possible:

i. Assuming transfer faults to be sub-linear and sub-vertical, they would have to transect topographical highs and cliff sides in the river valleys.

ii. Assuming transfer faults use basement weaknesses that are not necessarily linear, then transpression and/or transtension zones would be expected on certain fault locations where the accommodation leads to a strike-slip component.

On both cases mentioned above, clear structures would be expected to be observable inside the river valleys, and none were observed.

D. Fault tip structures described on Figure 30 may not exist or may not have an important role. This would support the interpretation that fault segment linkage is by transfer faults.

E. Recent unpublished master thesis work at University of Stavanger suggests evidence of a north-south transfer fault along the Vouraikos river valley (Figure 8).

Overall interpretation 2 (Figure 31) is a possibility for the area, but as gravity data is inconclusive by itself, and considering the Gulf of Corinth as a continental narrow rift, the information from analogs and experimental data suggest transfer faults to be uncommon on the area. This suggestion does not exclude the possibility and there are factors in favor of this interpretation, but the absence of knowledge about basement weaknesses and the lack of solid field observations does not allow for this interpretation to be entirely backed on this thesis.

3. A third possibility can be suggested using new field data (Figure 31 – Interpretation 03), where:

i. A basement exposure ahead of the Pirgaki segment has been mapped at 780m above sea level (Figure 24 and central map on Figure 31). This exposure is located on an area where Middle Group thickness was expected to be considerably high;

ii. A fault exposure was discovered behind what is commonly believed to be the main Mamousia segment (which is currently defined by a lithological change alone).

Considering the discussion shown on the geological background section, fault growth is initially related with isolated sub-parallel and scattered segments that link into major faults (Figure 3) (Cowie, 1998; Gawthorpe and Leeder, 2000). Observing the central map of Figure 31 two minor

interpretations can be made:

- The Mamousia segment can tip westward tending to link with the minor fault segment in front of the Pirgaki segment. Observations show that the basement exposure ahead of the Pirgaki segment is at 780m above sea level, and that basement is not exposed at the river valley level. Therefore the minor fault segment would have to tip eastward with a slope of at least 6% along the fault strike to allow for this interpretation (Figure 32). A mechanical interaction between segments can produce asymmetric D-L profiles that could help justify this 6% slope
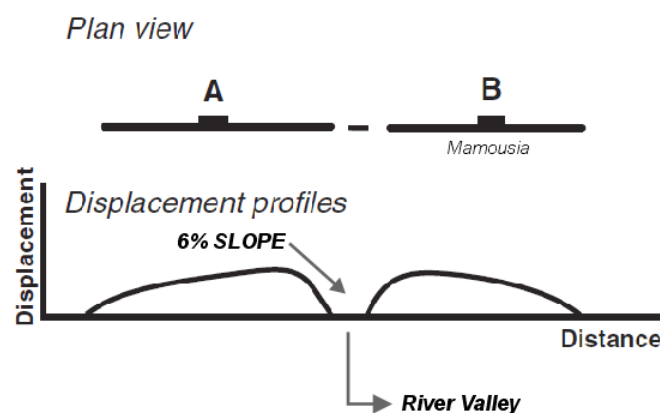
Figure 32 - Schematic displacement versus fault length (D-L) profiles modified from Gawthorpe and Leeder (2000). Segments A is supposed to simulate a fault related to the mapped basement exposure found in front of the Pirgaki segment. Segment B simulates the Mamousia segment. Asymmetric profiles indicate mechanical interaction between fault segments.

- The Eliki East segment could be tending to link with the well aligned minor fault segments behind the Eliki West.

With interpretation 03 (Figure 31) faults would cross the valley to tip or continue on either side. Unobserved fault tips could present structures that if present could aid segment interaction. These structures could also explain preferential weak zones where erosional processes can take place and steep valleys can be carved.

Although this interpretation allows for a better fit of field observations made, all fault tip structures are assumed, there are no field observations to support faults crossing river valleys, and there are no detailed observations on the Middle Group topsets that justify a 6% slope on the basement at that location.

From discussions of Figure 31, it is not possible to isolate an ideal interpretation as all of them rely heavily on assumptions and are weak on detailed field observations. That being said, interpretation 3 explains the mapped lithological distribution, provides an explanation for fault linkage and allows the construction of cross sections that are faithful to collected data. Lack of detailed observations can be attributed to the regional scale of the work.

As noticed from the previous discussions, knowledge related to the underling relief of the basement is poor, although pre-rift topography and syn-rift faulting is an important factor to study the overlying sediment depositional history. While these uncertainties influenciate further discussions related to thickness and distribution of sediment covers, the region can be reasonably divided as described in the literature between Basement, Lower Group, Middle Group and Upper Group (McNeill and Collier, 2004; Flotté et al., 2005; Ghisetti and Vezzani, 2005; McNeill et al., 2005; McNeill et al., 2007; Rettenmaier, 2007; Rohais et al., 2007; Benedicto et al., 2008; Ford et al., 2009; Backert et al., 2010; Leeder et al., 2012; Ford et al., 2013; Gobo, 2014b). Field observations were not focused on defining depositional environments, nonetheless one slight modification is suggested:

- The Lower Group has been defined mainly as fluvio-lacustrine facies, but the field observations point that thick packages of poorly sorted and immature conglomerates are abundant the south of the Mamousia-Pirgaki Fault, and these seem likely to be related to a stream dominated alluvial fan (Figure 25B). Therefore this unit should be more accurately defined as composed of transitions between alluvial, fluvial and lacustrine facies.

With this modification in mind, the following discussions can be made for the Lower Group:

1. No growth strata have been observed in the field. However the size of the outcrops (up to 200 meters) related to the possible size of the fan (15 kilometers) makes it possible that growth strata are not visible on our scale of observation. On kilometer scale exposures located outside the study area limits along the Vouraikos river valley (Figure 8), there is no clear evidence of grow strata patterns from observation points made along the road.

2. Also related to growth strata, stereograms show a 40° wide dip angle distribution in this unit (Figure 27). Inconclusive as it is, this might be the best indication of growth strata in the collected observations. More detailed studies would be necessary to differentiate growth

strata from sedimentological dip variations.

3. There is an possible regional trend defining this unit:

    a. Coarse alluvial sediments are associated with fluvial channels on the southern portion of the study area;

    b. Lacustrine sand and silt prone facies becomes more influential towards the north.

    Although data is poorly distributed and insufficient to support a confident interpretation, the observations may indicate that fans have proximal deposits on the south, extending approximately 15 kilometers towards the north and ending on distal lacustrine environments.

Literature on the Middle Group (Skourtsos and Kranis, 2009; Ford et al., 2013; Gobo, 2014b; Hemelsdaël and Ford, 2015) is in accordance with field observations. Regardless of similarities with literature, few discussions can still be made:

1. Topsets generally dip gently southward as described on Figure 27. This is a clear indication that the fault blocks have been slightly rotated.

2. The current topographical location of the highest mapped topsets is 800 meters above sea level (Figure 28). This uplift is not on the same scale order as the 1800 meters of regional uplift described on the literature. Local erosion as well as the lack of control over eustatic variations may affect the apparent observed uplift in relation to values presented by the literature (Skourtsos and Kranis, 2009; Hemelsdaël and Ford, 2015).

3. The Middle Group deltas are clearly cut by the Eliki Fault segments indicating a time relation between this sedimentological unit and the Eliki Fault system faulting.

4. Delta development and sedimentation has been an constant factor in the region as older uplifted deltas locally transition to younger systems (e.g. Kouloura > Aigio, Platanos > Akrata) as shown on Figure 20.

5. Stereograms show a 60° wide dip angle distribution for the topsets of this unit (Figure 27). This scattering can be related to the fact that topsets of different delta units have been

gathered on a single stereogram. Uneven uplift and fault block rotation patterns associated with different depositional system geometries of these different sedimentary units are probable factors that influenciate scattering of measurements.

6. Mostly topsets dip southwards with lesser east and west components, while limited dip angles are sub-horizontal and northward dipping (Figure 27). South dipping topsets are to be expected with fault block rotation, and the few north dipping layers are possibly related to the transition area between topsets and foresets as can be observed on the Kerinitis Delta (Figure 16 and Figure 28).

The Upper Group was not observed on outcrop level to support detailed discussions. With aid of Figure 20, the above sea level sedimentation patterns can be observed for the Upper Group deltas and few discussions are possible:

1. The Aigio Delta paleo channel pattern indicates an eastward migration trend. This is most likely related to the uplift caused by the eastward tip migration of the active Eghio Fault (Figure 20 and Figure 33).

2. Delta shapes as highlighted Figure 20 indicate these depositional systems are mostly wave dominated.

3. The presence of marine terraces seems to be concentrated on regions where the rift is wider. This might suggest that steep slopes and no marine terraces were present on initial stages of the rift.

Figure 33 - Google Earth satellite image integrated with DEM (Google, 2015b) showing a sketch of relations between mapped structural, lithological and geomorphological features. Main points to be highlighted are: (i) Structural interpretation derived from field data with generalized fault footwall exposure; (ii) Simplified lithological compartmentalization with dominant units for each region; (iii) Relay ramp influence on development on sedimentation paths shown as red dotted arrows.

Figure 33 summarizes well the relationships between modern (Upper Group) and uplifted (Middle Group) deltas related to fault development. Observing the clear relation between recent deltas and active recent faults might be the key to understand the uplifted deltas and older inactive major faults in the region. From the interpretation made over Figure 33 it is important to highlight:

- The Eghio Fault main segment is followed by multiple smaller fault segments to the south. This supports Cowie (1998) fault evolution suggestion (Figure 3) that has been repeatedly used on this thesis.

- Although the Eghio Fault topographically seems to tip inland, bathymetric data brought by McNeill et al. (2007) shows clear evidence that multiple fault segments are present under water. This suggests that faults do not always influenciate syn-rift sediments clearly at the observable surface. Therefore attention should be taken when interpreting fault tips when cover sediments do not show evidence of faulting.

- A relay ramp seems to develop between the Eliki West and the Eghio Fault segments. This ramp develops a slope that controls paleo channel directions and consequently the Aigio Delta shape. It is reasonable to assume that Middle Group deltas should occasionally show similar patterns.

- The interpretation on DEM topography and satellite images on the Eliki Fault system allows for definition of multiple parallel fault segments. These segments generally right step while their tips show a considerable overlap. This interpretation supports Figure 31 Interpretation 3, and although it is in accordance with field observations, a relay ramp in this location is unlikely due to the steepness of the slope and abruptness of changes. These factors may indicate that if a ramp existed, it might have been breached.

Geological profiles

Geological profiles are a good tool to spot inconsistencies on geological maps, allow for displacement estimation and calculate sediment cover thickness.

Based on all field observations, interpretations discussed on this section and the geological map of Figure 16, profiles transecting the main structures of the area were constructed and are displayed on Figure 34 as:

- Five profiles (A-B, C-D, E-F, G-H and I-J) show a parallel cut over the general dip direction;

- One extensive profile (K-L) along the regional fault strike direction attempts to connect the previous profiles over areas with poorly constrained field data.

The profiles of Figure 34 attempt to be consistent with field observations, however uncertainties are present and can be summarized as:

- Fault connectivity along strike is commonly uncertain;

- There is little to no control over intra-block faulting on areas where syn-rift sediments are present;

- The extent, thickness and continuity of the Lower Group under the Middle Group is frequently unknown;

- Although the existence of the Middle Group under the Upper Group can be expected, its extent and continuity is unknown and will be omitted from profiles.

- The along fault strike profile K-L on Figure 34 present syn-rift thickness and contact information only at intersection marker locations.

- The thrust faults in the basement unit shown on profile K-L on Figure 34 are an illustrative interpretation that is not based on field data, but only on the regional geology information, and therefore no attempt is intended on defining thin or thick-skinned deformation as more information would be needed
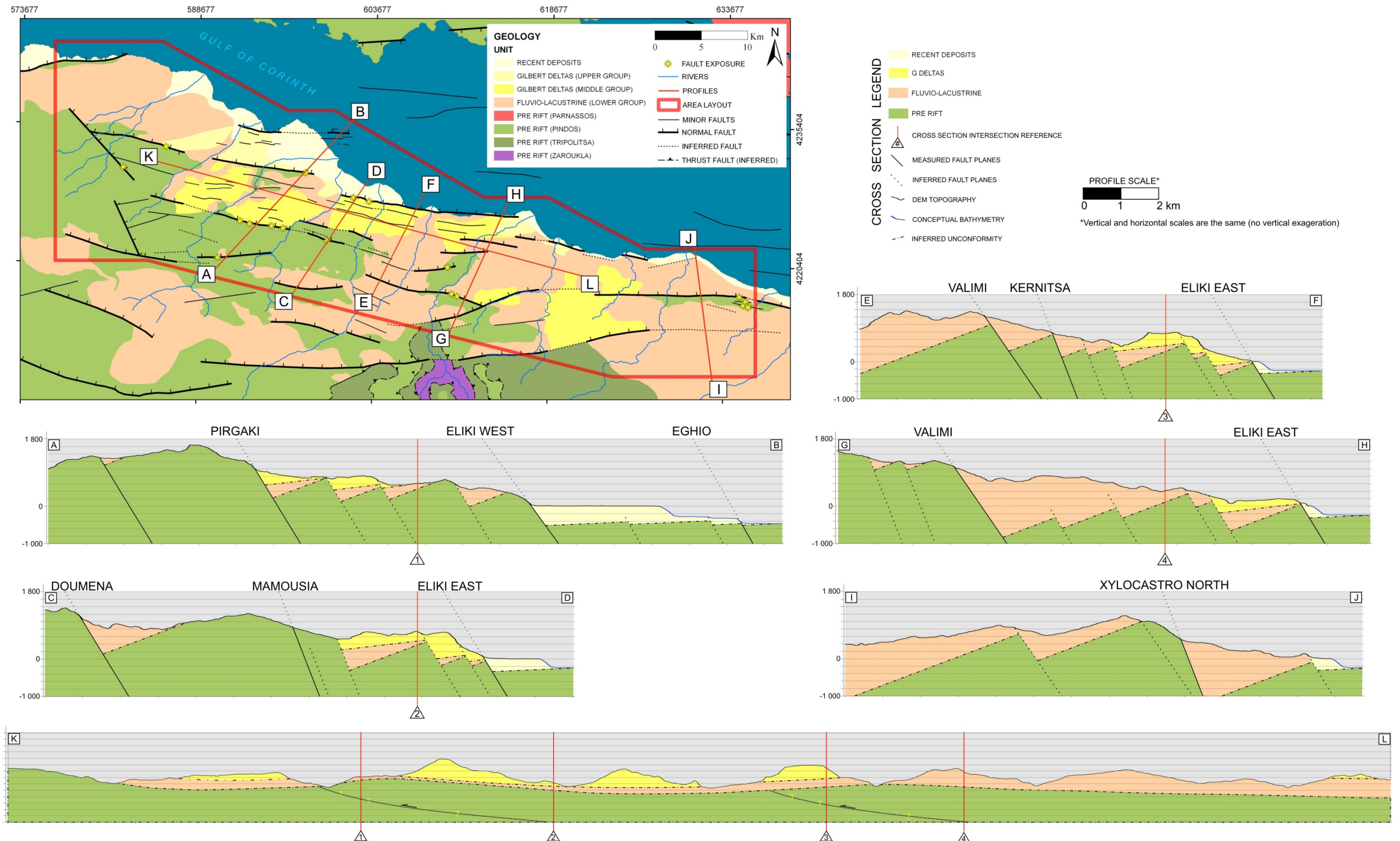
Figure 34 – Geological profiles transecting key features mapped on the field. Profiles A-B, C-D, E-F, G-H and I-J are perpendicular to the major structures in the mapped area, while profile K-L is along strike to these structures. The intersection between sections is indicated by markers that are adequately positioned and numbered to facilitate correlations. Profile K-L attempts to connect poorly constrained locations and shows an interpretation for pre-rift basement topographical variations that supports the lateral variations seen on other profiles. On K-L profile thrust faults are represented as an optional interpretation based on regional geology knowledge, and it is important to note that no observations have been made to support thin or thick skinned interpretations, and therefore represented fault are purely illustrative of an option.

Displacements

Displacements are calculated based on geological profiles, remote sensor datasets and the field observations. For segments described on Figure 23, fault displacements estimates are summarized on Table 3. For interpreted fault segments that were not directly observed on the field, estimates are summarized on Table 4. Calculated displacement locations can be referenced on Figure 35.
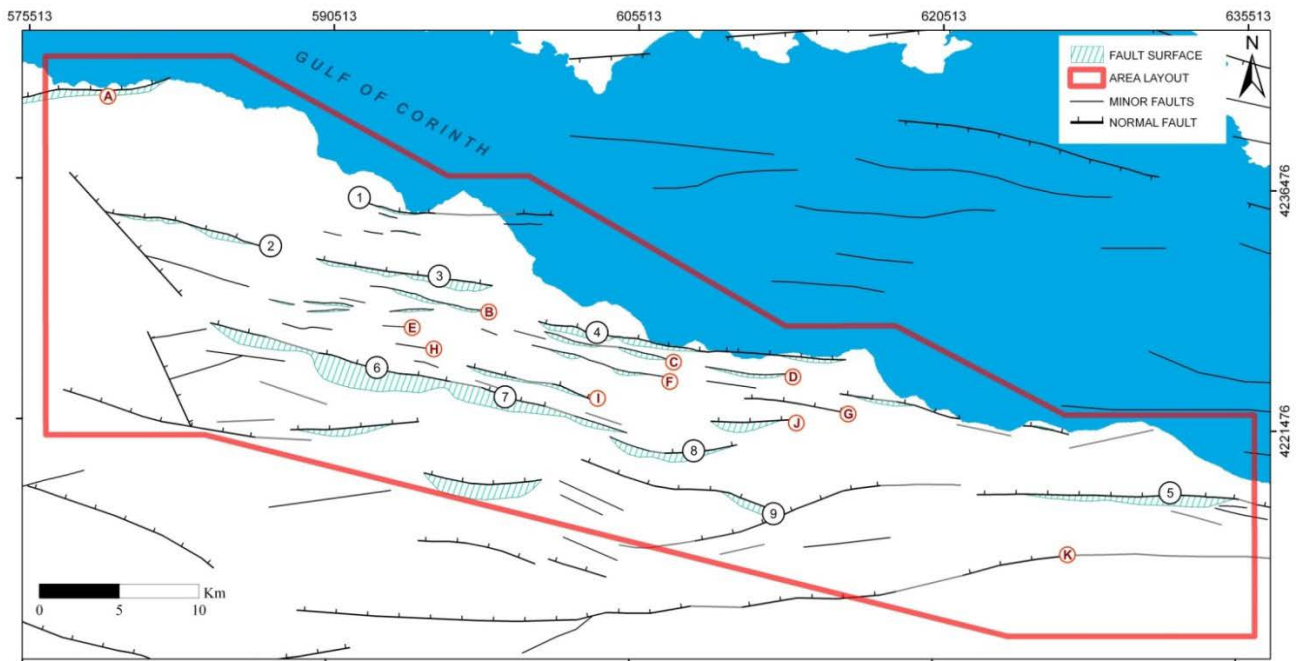
Figure 35 - Location map of displacement estimates supporting Table 3 and Table 4

Table 3 –Displacement summary for mapped faults containing values derived from different methods (in meters).
*   Calculation done assuming hanging wall is downthrown as much as footwall is uplifted.
**   The Eghio Fault estimation is has been derived based on data from Place et al. (2007).

	FAULT	SEGMENT	SEGMENT DIP CYLINDRICAL BEST FIT	TOPOGRAPHY MAX VERTICAL TOPOGRAPHICAL DIFFERENCE	DISPLACEMENT			
					ESTIMATE BASED ON TOPOGRAPHY AND BEST FIT FAULT DIP *	MOST LIKELY VALUE BASED ON LOCAL DATA CLOSE TO FAULTS	MINIMUM BASED ON REGIONAL DATA	MAXIMUM BASED ON REGIONAL DATA
1	LAKKA	---	51	498	1282	---	1190	1780
2	EGHIO**	---	60	100	231	230	---	---
3	ELIKI	WEST	54	721	1782	---	1205	---
4	ELIKI	EAST	59	485	1132	---	395	---
5	XYLOCASTRO	NORTH	70	899	1913	---	1850	2420
6	MAMOUSIA-PIGARKI	PIGARKI	59	1330	3103	2800	2440	4200
7	MAMOUSIA-PIGARKI	MAMOUSIA	69	1030	2207	2108	1335	3730
8	KERINITIS	---	69	742	1590	---	870	2750
9	VALIMI	---	56	800	1930	---	2300	4700

Table 4 - Displacement summary for interpreted fault segments that were not observed directly containing values derived from different methods (in meters).

INTERPRETED FAULT SEGMENTS	SEGMENT DIP ASSUMED VALUES BASED ON NEIGHBOUR FAULTS	TOPOGRAPHY MAX VERTICAL TOPOGRAPHICAL DIFFERENCE	DISPLACEMENT		
			ESTIMATE BASED ON TOPOGRAPHY AND ASSUMED FAULT DIP	MINIMUM BASED ON PROFILE INTERPRETATION	MAXIMUM BASED ON PROFILE INTERPRETATION
A	55	310	757	---	---
B	54	191	472	910	910
C	59	100	233	0	618
D	69	---	---	671	1475
E	59	---	---	0	407
F	59	265	618	0	1183
G	69	218	467	430	1815
H	59	---	---	615	1150
I	69	404	865	1416	3630
J	69	140	300	280	348
K	70	457	973	0	1044

All the displacements shown on Table 3 and Table 4 contain uncertainties as estimates are based on profiles that rely on assumptions such as:

- Unconformities are flat and no pre-rift inherited paleo topography exists;
- Unconformities dip parallel to overlying syn-rift layers;
- Syn-rift units have an uncertain extent over certain areas;
- Regional data used for syn-rift dip where local measurements were not available.

The sketch of Figure 33 added with the displacement values estiamted is shown on Figure 36. From these displacement relations the following interpretations are deduced:

- There is a westward displacement decrease from the Pigarki towards the Kernitis segment;
- Considering Interpretation 3 Figure 31, the Eliki East segment tips eastward towards the "B" segment (Table 4)
- The Eliki West possibly tips westwards.
- In general the southern segments Pigarki, Mamousia, Kerinitis and Valimi have higher displacements when compared to the northern segments Eliki East, Eliki West, Lakka, Xylokastro and Eghio.
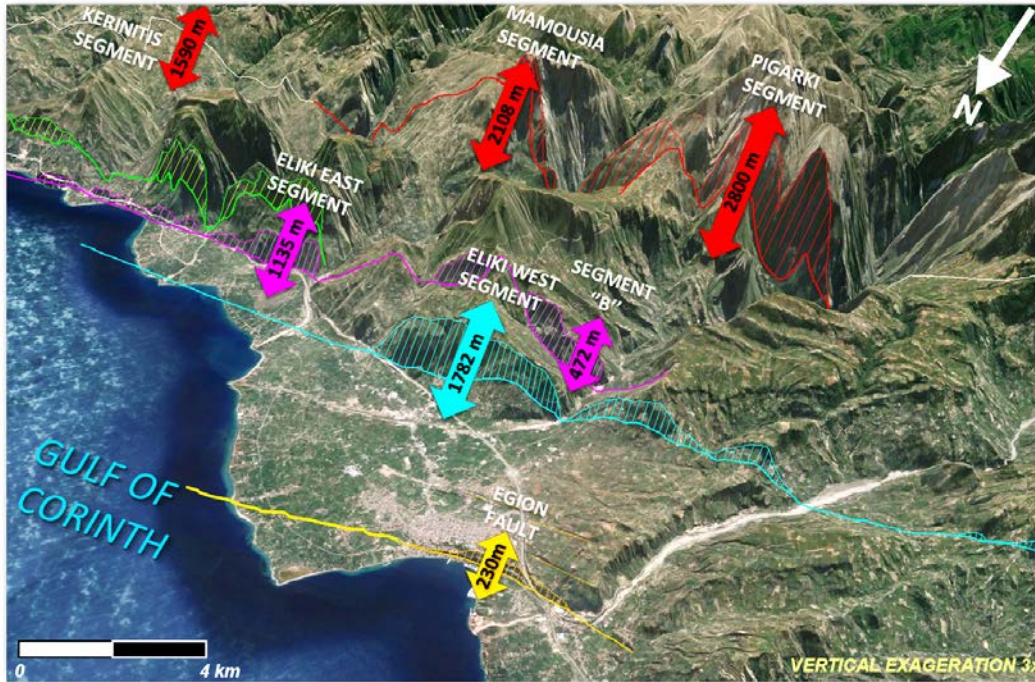
Figure 36 - Google Earth satellite image integrated with DEM (Google, 2015b) showing a sketch of relations between displacement estimates and structural features. Values are obtained from Table 3 and Table 4 using topographic derived values for all faults besides the Eghio, Mamousia and Pirgaki which display most likely values.

To compare, test and integrate the discussions related to rotated fault blocks with calculated displacement values (Table 3 and Table 4) and the statically derived regional dip angles for sediment units (Figure 27), a test has been attempted based on the following assumptions:

- Considering the Mamousia-Pirgaki and the Eliki faults the bounding structures of a rotated fault block, this block would be approximately 8 kilometers long (Figure 37);
- Assuming that intra block faulting is not significant;
- Assuming the Middle Group topsets to be deposited as sub horizontal layers;

With the above simplifications and using simple trigonometry, it is possible to obtain a rough estimate of 1000 meters displacement for the Pirgaki segment so that topsets are rotated 7° southward.

The discrepancy between the resulting 1000 meters displacement from the above test compared with calculated most likely values of 2800 meters (Table 3) indicate that the assumptions made are not correct. And by analyzing the assumptions, a likely answer is that intra-block faults play an important part on sharing the displacement within the fault block.
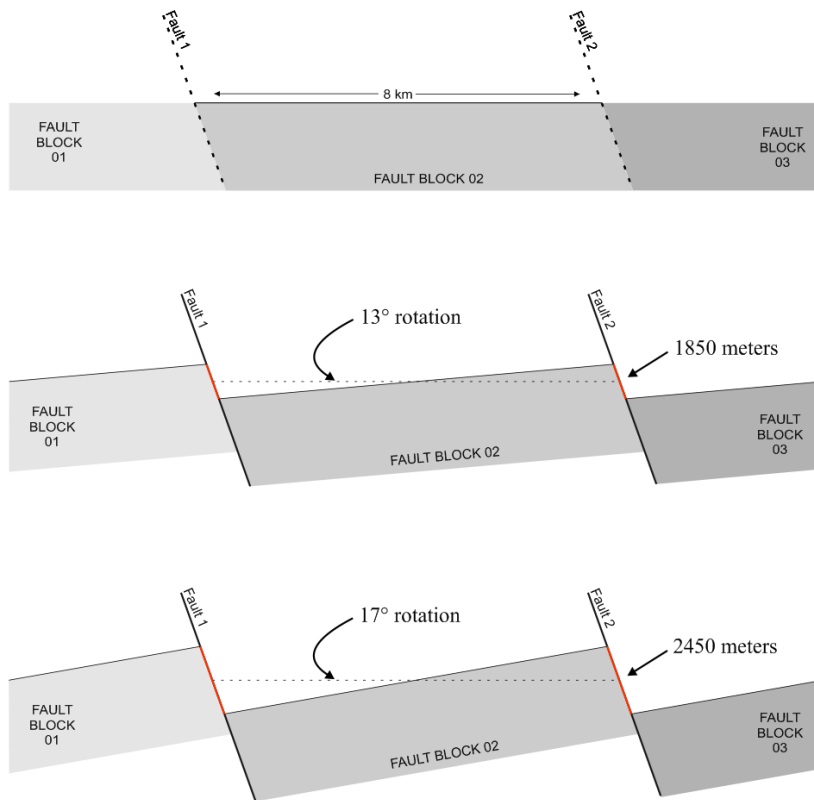
Figure 37 – Relation between fault block rotation and fault displacement.

CONCLUSIONS

1. Neighboring major fault segments are likely to present a mechanical interaction over hard and/or soft linked structures. These aligned fault segment arrays seems to act regionally as single faults that can extend for up to 50 kilometers on a predominant S75°E direction.

2. Major fault segments extend up to 10 kilometers long and can contain a fault damage zone that is up to 100 meters wide. These zones contain multiple discrete brittle structures and show no clear evidence of ductile deformation.

3. An array of relatively small faults is clearly visible to the south of the active Eghio Fault. This faulting pattern associated with a main active fault can be expected to play an important role on the surroundings of all other major fault systems in the study area. It is important to notice that syn-rift sedimentary covers are known to omit clear evidence of such faulting when displacements are or tend to become low.

4. "Most Likely" displacement values were obtained only for the Mamousia, the Pirgaki and the Eghio faults with respectively 2108, 2800 and 230 meters. The Lakka fault presents estimates ranging between 1190 to 1780 meters, the Xylokastro North Fault ranges between 1850 and 2420 meters and the Eliki West Fault is estimated between 1205 and 1782. All other fault segments present large uncertainty on estimated values.

5. Fault displacements vary on scales of hundreds to thousands of meters. Estimates indicate a general trend where southern faults have higher displacement than northern faults, as well as eastern segments have higher displacements than western segments.

6. Kinematic indicators on the form of slickenside lineaments indicate that normal and oblique fault slips are related to fault development in the region.

7. The coastal fault history is closely related to the Middle and Upper group development and architecture. The same relations with the Lower Group can be expected although data obtained is not adequate to allow detailed interpretations as this unit extends considerably outside of the study area.

8. Following the evolution pattern in the region with younger faults developing northwards and fault tips migrating westwards, delta and paleo channel architectures of the Middle Group may be predicted by observing modern patterns observable on the Upper Group.

REFERENCES

Acocella, V., P. Morvillo, and R. Funiciello, 2005, What controls relay ramps and transfer faults within rift zones? Insights from analogue models: Journal of Structural Geology, v. 27, p. 397-408.

Athmer, W., and S. M. Luthi, 2011, The effect of relay ramps on sediment routes and deposition: A review, p. 1-17.

Backert, N., M. Ford, and F. Malartre, 2010, Architecture and sedimentology of the Kerinitis Gilbert-type fan delta, Corinth Rift, Greece: Sedimentology, v. 57, p. 543-586.

Benedicto, A., V. Plagnes, P. Vergély, N. Flotté, and R. A. Schultz, 2008, Fault and fluid interaction in a rifted margin: Integrated study of calcite-sealed fault-related structures (southern Corinth margin), Geological Society Special Publication, p. 257-275.

Cornet, F. H., M. L. Doan, I. Moretti, and G. Borm, 2004, Drilling through the active Aigion Fault: the AIG10 well observatory: Comptes Rendus Geoscience, v. 336, p. 395-406.

Cowie, P. A., 1998, A healing–reloading feedback control on the growth rate of seismogenic faults: Journal of Structural Geology, v. 20, p. 1075-1087.

Daniel, J.-M., I. Moretti, L. Micarelli, S. E. Chuyne, and C. D. Piane, 2004, Macroscopic structural analysis of AG10 well (Gulf of Corinth, Greece): Comptes Rendus Geoscience, v. 336, p. 435-444.

De Martini, P. M., D. Pantosti, N. Palyvos, F. Lemeille, L. McNeill, and R. Collier, 2004, Slip rates of the Aigion and Eliki Faults from uplifted marine terraces, Corinth Gulf, Greece: Comptes Rendus - Geoscience, v. 336, p. 325-334.

Doblas, M., V. Mahecha, M. Hoyos, and J. López-Ruiz, 1997, Slickenside and fault surface kinematic indicators on active normal faults of the Alpine Betic Cordilleras, Granada, southern Spain: Journal of Structural Geology, v. 19, p. 159-170.

Doutsos, T., and I. Koukouvelas, 1998, Fractal analysis of normal faults in northwestern Aegean area, Greece: Journal of Geodynamics, v. 26, p. 197-216.

Esri, 2012, ArcGIS (v. 10.1), Environmental Systems Research Institute, licensed to University of Stavanger.

Esri, 2014, World Imagery Mosaic scene (DigitalGlobe, GeoEye, i-cubed, Earthstar Geographics, CNES/Airbus DS,USDA, USGS, AEX, Getmapping, Aerogrid, IGN, IGP, swisstopo, and the GIS User Community), Mosaic, ArcMap™, ArcGIS® software by Esri, Unknown Acquisition Dates.

Etheridge, M. A., 1986, On the reactivation of extensional fault systems: Philosophical Transactions - Royal Society of London, Series A, v. 317, p. 179-194.

Flotté, N., D. Sorel, C. Müller, and J. Tensi, 2005, Along strike changes in the structural evolution over a brittle detachment fault: Example of the Pleistocene Corinth-Patras rift (Greece): Tectonophysics, v. 403, p. 77-94.

Ford, M., S. Rohais, E. A. Williams, S. Bourlange, D. Jousselin, N. Backert, and F. Malartre, 2013, Tectono-sedimentary evolution of the western Corinth rift (Central Greece): Basin Research, v. 25, p. 3-25.

Ford, M., E. A. Williams, F. Malartre, and S.-M. Popescu, 2009, Stratigraphic Architecture, Sedimentology and Structure of the Vouraikos Gilbert-Type Fan Delta, Gulf of Corinth, Greece, Sedimentary Processes, Environments and Basins, Blackwell Publishing Ltd., p. 49-90.

Gawthorpe, R. L., and M. R. Leeder, 2000, Tectono-sedimentary evolution of active extensional basins: Basin Research, v. 12, p. 195-218.

Géraud, Y., M. Diraison, and N. Orellana, 2006, Fault zone geometry of a mature active normal

fault: A potential high permeability channel (Pirgaki fault, Corinth rift, Greece): Tectonophysics, v. 426, p. 61-76.

Ghisetti, F., and L. Vezzani, 2005, Inherited structural controls on normal fault architecture in the Gulf of Corinth (Greece): Tectonics, v. 24, p. 1-17.

Giba, M., J. J. Walsh, and A. Nicol, 2012, Segmentation and growth of an obliquely reactivated normal fault: Journal of Structural Geology, v. 39, p. 253-267.

Gobo, K., 2014a, Development of Gilbert-type deltas: sedimentological case studies from the Plio-Pleistocene of Corinth Rift, Greece: Ph.D. thesis, University of Bergen.

Gobo, K., 2014b, Development of Gilbert-type deltas: sedimentological case studies from the Plio-Pleistocene of Corinth Rift, Greece: Doctoral thesis thesis, University of Bergen, 121 p.

Google, 2015a, Google Earth Pro (v. 7.1.2.2041), Google Earth Pro, licensed

Google, 2015b, Imagery Mosaic scene (CNES/Astrium, Digital Globe, Landsat, SiO, NOAA, U.S. Navy, NGA, GEBCO, LDEO-Comlumbia, NSF, TerraMetrics), GoogleEarthPro® software by Google, Unknown Acquisition Dates.

Gudmundsson, A., G. De Guidi, and S. Scudero, 2013, Length–displacement scaling and fault growth: Tectonophysics, v. 608, p. 1298-1309.

Hatzfeld, D., V. Karakostas, M. Ziazia, I. Kassaras, E. Papadimitriou, K. Makropoulos, N. Voulgaris, and C. Papaioannou, 2000, Microseismicity and faulting geometry in the Gulf of Corinth (Greece): Geophysical Journal International, v. 141, p. 438-456.

Hemelsdaël, R., and M. Ford, 2015, Relay zone evolution: A history of repeated fault propagation and linkage, central Corinth rift, Greece: Basin Research.

Hirt, C., S. Claessens, T. Fecher, M. Kuhn, R. Pail, and M. Rexer, 2013, New ultrahigh-resolution picture of Earth's gravity field: Geophysical Research Letters, v. 40, p. 4279-4283.

Kim, Y.-S., and D. J. Sanderson, 2005, The relationship between displacement and length of faults: a review: Earth-Science Reviews, v. 68, p. 317-334.

Koukouvelas, I. K., L. Stamatopoulos, D. Katsonopoulou, and S. Pavlides, 2001, A palaeoseismological and geoarchaeological investigation of the Eliki fault, Gulf of Corinth, Greece: Journal of Structural Geology, v. 23, p. 531-543.

Leeder, M. R., G. H. Mack, A. T. Brasier, R. R. Parrish, W. C. McIntosh, J. E. Andrews, and C. E. Duermeijer, 2008, Late-Pliocene timing of Corinth (Greece) rift-margin fault migration: Earth and Planetary Science Letters, v. 274, p. 132-141.

Leeder, M. R., D. F. Mark, R. L. Gawthorpe, H. Kranis, S. Loveless, N. Pedentchouk, E. Skourtsos, J. Turner, J. E. Andrews, and M. Stamatakis, 2012, A "Great Deepening": Chronology of rift climax, Corinth rift, Greece: Geology, v. 40, p. 999-1002.

McClay, K., and S. Khalil, 1998, Extensional hard linkages, eastern Gulf of Suez, Egypt: Geology, v. 26, p. 563-566.

McNeill, L. C., and R. E. L. Collier, 2004, Uplift and slip rates of the eastern Eliki fault segment, Gulf of Corinth, Greece, inferred from Holocene and Pleistocene terraces: Journal of the Geological Society, v. 161, p. 81-92.

McNeill, L. C., R. E. L. Collier, P. M. De Martini, D. Pantosti, and G. D'Addezio, 2005, Recent history of the Eastern Eliki Fault, Gulf of Corinth: Geomorphology, palaeoseismology and impact on palaeoenvironments: Geophysical Journal International, v. 161, p. 154-166.

McNeill, L. C., C. J. Cotterill, J. M. Bull, T. J. Henstock, R. Bell, and A. Stefatos, 2007, Geometry and slip rate of the Aigion fault, a young normal fault system in the western Gulf of Corinth: Geology, v. 35, p. 355-358.

Micarelli, L., I. Moretti, and J. M. Daniel, 2003, Structural properties of rift-related normal faults: The case study of the Gulf of Corinth, Greece: Journal of Geodynamics, v. 36, p. 275-303.

Micarelli, L., I. Moretti, M. Jaubert, and H. Moulouel, 2006, Fracture analysis in the south-western

Corinth rift (Greece) and implications on fault hydraulic behavior: Tectonophysics, v. 426, p. 31-59.

Moretti, I., D. Sakellariou, V. Lykousis, and L. Micarelli, 2003, The Gulf of Corinth: An active half graben?: Journal of Geodynamics, v. 36, p. 323-340.

Morley, C. K., R. A. Nelson, T. L. Patton, and S. G. Munn, 1990, Transfer zones in the East African rift system and their relevance to hydrocarbon exploration in rifts: American Association of Petroleum Geologists Bulletin, v. 74, p. 1234-1253.

Mrlina, J., 2014, Do active transverse faults exist on the southern coast of Corinth rift?: Near Surface Geoscience 2014 - 20th European Meeting of Environmental and Engineering Geophysics.

Papanikolaou, D., 2013, Tectonostratigraphic models of the Alpine terranes and subduction history of the Hellenides: Tectonophysics, v. 595-596, p. 1-24.

Papanikolaou, D. J., and L. H. Royden, 2007, Disruption of the Hellenic arc: Late Miocene extensional detachment faults and steep Pliocene-Quaternary normal faults - Or what happened at Corinth?: Tectonics, v. 26.

Pavlides, S. B., I. K. Koukouvelas, S. Kokkalas, L. Stamatopoulos, D. Keramydas, and I. Tsodoulos, 2003, Late Holocene evolution of the East Eliki fault, Gulf of Corinth (Central Greece): Quaternary International, v. 115-116, p. 139-154.

Peacock, D. C. P., 2002, Propagation, interaction and linkage in normal fault systems: Earth-Science Reviews, v. 58, p. 121-142.

Peacock, D. C. P., R. J. Knipe, and D. J. Sanderson, 2000, Glossary of normal faults: Journal of Structural Geology, v. 22, p. 291-305.

Place, J., C. Naville, and I. Moretti, 2007, Fault throw determination using 4 component VSP: Aigion fault (Greece) case study: Tectonophysics, v. 440, p. 141-158.

Rettenmaier, D., 2007, Thermo-hydraulic conditions in a seismically active zone (Gulf of Corinth,Greece): Doctoral thesis thesis, Universität Fridericiana zu Karlsruhe, 162 p.

Rohais, S., R. Eschard, M. Ford, F. Guillocheau, and I. Moretti, 2007, Stratigraphic architecture of the Plio-Pleistocene infill of the Corinth Rift: Implications for its structural evolution: Tectonophysics, v. 440, p. 5-28.

Sandwell, D. T., R. D. Müller, W. H. F. Smith, E. Garcia, and R. Francis, 2014, New global marine gravity model from CryoSat-2 and Jason-1 reveals buried tectonic structure: Science, v. 346, p. 65-67.

Skourlis, K., and T. Doutsos, 2003, The Pindos Fold-and-thrust belt (Greece): Inversion kinematics of a passive continental margin: International Journal of Earth Sciences, v. 92, p. 891-903.

Skourtsos, E., and H. Kranis, 2009, Structure and evolution of the western Corinth rift, through new field data from the northern Peloponnesus, Geological Society Special Publication, p. 119-138.

Taylor, B., J. R. Weiss, A. M. Goodliffe, M. Sachpazi, M. Laigle, and A. Hirn, 2011, The structures, stratigraphy and evolution of the Gulf of Corinth rift, Greece: Geophysical Journal International, v. 185, p. 1189-1219.

USGS-METI, 2011, ASTER Global DEM scene ASTGDEMV2_0N38E021+0N37E021+0N38E022+0N37E022, Stereo-correlated and Stacked, NASA LP DAAC & METI ERSDAC, Sioux Falls-United States, 17/10/2011.

USGS, 2014, Landsat 8 OLI/TIRS scene LC81840342014242LGN00, Pre-WRS-2, NASA Landsat Program, Sioux Falls-United States, 30/08/2014.

WACG, 2014, GGMplus (Global Gravity Model Plus) scene N35E020, Gravity Disturbance, Western Australian Center of Geodesy (Curtin University), Perth-Australia, 30/08/2014.